Hierarchical Petri Nets for Modeling Metabolic Phenotype in Prokaryotes

N. Balasubramanian,[†] Ming-Li Yeh, and Chuei-Tin Chang*

Department of Chemical Engineering, National Cheng Kung University, Tainan, Taiwan 70101, ROC

Shu-Jen Chen

Department of Chemical and Material Engineering, National Kaohsiung University of Applied Sciences, Kaohsiung, Taiwan 80778, ROC

A systematic strategy is presented in this paper to build Petri-net models for the biological reaction networks and their gene regulation mechanisms in prokaryotes. Component models are first developed to represent the cellular functional units, i.e., operons, regulons, modulons, and individual reactions. A step-by-step procedure is then proposed to assemble these components to form hierarchical system models. The usefulness of the proposed approach is demonstrated with a realistic example. The model validity is shown by comparing simulation predictions with experimental data in the literature.

1. Introduction

As a result of recent advancement in biotechnology, it is now a popular practice to improve cellular properties via gene modification. The regulatory mechanisms of genes can often be altered to promote the enzyme activities, to extend metabolic reaction pathways, and/or to create new arrays of enzymes for the production of novel molecules. To facilitate implementation of this approach, extensive studies have been performed in a newly evolved research field, Metabolic Engineering. Bailey[1] suggested that its activities could be characterized as the improvement of cellular activities by manipulations of enzymatic, transport, and regulatory functions of the cell with the use of recombinant DNA technology. Numerous books and reviews have already been published in the literature, e.g., Stephanopoulos et al.,[2] Stephanopoulos,[3] Nielsen et al.,[4] Lengeler,[5] etc. Generally speaking, application of the metabolic engineering methods always starts with a careful analysis of cellular functions and then an improved strain is developed according to a given design objective.[4] A large number of examples can be found in the literature and some of them are briefly outlined below: Porro et al.[6] improved the lactic acid production process by incorporating mammalian lactate dehydrogenase in *Saccharomyces cerevisiae* through molecular modification. Flares et al.[7] isolated new *Escherichia coli* strains to facilitate glucose transport without phosphoenolpyruvate (PEP). Millard et al.[8] reported enhanced succinate production in *E. coli* by the overexpression of PEP carboxylase. Finally, a microbial process was developed by Yang et al.[9] to produce indigo and propylene glycol.

It is obvious that the development of a workable model is a key step in the analysis of any metabolic phenotype.[10] The traditional mathematical modeling tools (i.e., the algebraic and differential equations) have long been used in many previous studies. The fluxes through different branches of a biochemical reaction network can be determined on the basis of metabolite balance[2]. Varma et al.[11] used a flux-balance-based formulation to study the synthesis of 20 amino acids and four nucleotides as the products of biochemical reactions. Also, a linear program was developed in a separate study to determine the optimal metabolic performance of *E. coli* under various oxygen limitations.[12] Hatzimanikatis et al.[13] proposed a mixed-integer linear programming (MILP) formulation for maximizing the performance of a given metabolic network. On the basis of experimental data, Lin et al.[14] also adopted a MILP model to identify the network topology of the glucose signaling pathway in yeast and also the role of Ras components in this network. Fell[15] used metabolic control analysis (MCA) to determine the elastic coefficients in the metabolic network. A quantitative model describing penicillin synthesis in *Penicillium chrysogenum* was used to predict the control and elasticity coefficients.[16] Ramakrishna et al.[17] used flux balance analysis (FBA) to characterize the optimal flux distributions for maximum ATP production in the mitochondrion. Jamshidi et al.[18] developed a Mathematica application package to perform dynamic simulation for the metabolic network in red blood cell (RBC). Kremling et al.[19−21] constructed equation-based software for analyzing the biochemical reaction networks with control mechanisms. In this software, each cellular activity is characterized as a functional unit and each unit is modeled with a set of mathematical equations. Finally, Schuster et al.[22] proposed a decomposition algorithm for analyzing the metabolic network pathways.

The main drawback of equation-based models is that they are not suitable for describing discrete events in the gene regulation processes.For example, according to the well-established mechanism of inducible expression, the transcriptional activity is turned on in the presence of inducer and off if otherwise. In addition, although the kinetic parameters in the rate equations of many metabolic reactions are readily available in the literature, most gene transcription and translation processes can only be described qualitatively. A graphi-

* To whom correspondence should be addressed. Tel: 886-6-275-7575, ext. 62663. Fax: 886-6-234-4496. E-mail: ctchang@mail.ncku.edu.tw.

[†] Permanent address: Central Electrochemical Research Institute, Karaikudi-630 006, Tamilnadu, India.

10.1021/ie049772k CCC: $30.25
Published on Web 03/01/2005

cal modeling tool, Petri net (PN), has thus been adopted as an alternative in some of the studies reported in the literature. As they were originally designed, the Petri-net models are most suitable for describing the discrete-event systems. Furthermore, one of the critical features of Petri net is its natural support for integrating a mix of quantitative and qualitative component models. Under the condition that some of the needed kinetic data for numerical simulation are missing, such a hybrid system model is believed to be more mechanistically sound when compared with the empirical correlations often adopted in the traditional modeling approach. Thus, although the predictions of this model may not be quantitatively accurate, they can be useful for validating a hypothesized mechanism and/or directing possible future experiments. Finally, to construct a comprehensible model of the gene regulation mechanisms, it is important not only to establish the unsteady-state material balances of proteins and metabolites but also to *explicitly* express the causal relationships between conditions and events in the system. To this end, the Petri nets are well equipped to depict a precise picture of these relationships in a complex metabolic network.

There have been many attempts in the past to use the Petri nets to model various metabolic systems. Reddy et al.[23] tried to treat the biochemical reaction networks as discrete-event systems. In their Petri-net model, the places denote the states of metabolites and transitions represent chemical reaction steps. Since only the stoichiometry of the reaction system is described, their analysis was limited to the qualitative aspects of the metabolic phenotype. Hofestädt and Thelen[24] extended this pioneering work by incorporating quantitative kinetic data with the continuous places in a hybrid Petri net. The token number in a continuous place represents the actual concentration of a metabolite, and the weight on the input or output arc of a transition represents the corresponding reaction rate. Koch et al.[25] also studied the pentose phosphate reaction cycle using a time-dependent Petri net, while Genrich et al.[26] proposed to use Petri-net models for the analysis of biochemical pathways. In addition to the studies on reaction dynamics, the Petri nets can also be used to describe the gene regulation mechanisms. Goss and Peccoud[27] proposed a stochastic Petri-net model for the protein synthesis process. Matsuno et al.[28] also developed a hybrid Petri net for the same purpose. The states of RNA polymerases were represented with discrete places, and those of enzymes and mRNAs with continuous places. The production and degradation rates of each protein are described with two separate continuous transitions. Although the Petri-net models developed in this work are quite useful, their model construction procedure is mostly ad hoc in nature. It is thus difficult for a novice to build a suitable model for new applications. Also, since the inherent hierarchical framework of signal flows in a cellular system is not clearly reflected in their model, their Petri nets cannot be easily read and understood. Finally, it should be noted that the collection of component models in this work is far from comprehensive. For example, Petri nets representing various functional units in prokaryotes, such as the modulons, regulons, and repressible operons, are ignored completely.

To facilitate the application of metabolic engineering methods, an *integrated* PN model is clearly required to predict the effects created by any change in the gene regulation behaviors. Although a good amount of studies on modeling of the gene regulated metabolic phenotype can be found in the literature,[29] the task of model construction at the present stage is still considered to be an art. The objective of the present investigation is thus to develop a systematic procedure to assemble a Petri net for modeling both the metabolic reactions and their regulatory mechanisms in any cell. To better illustrate the proposed model building procedure, the scope of the present paper is limited to the metabolic phenotype in prokaryotes. It should be emphasized that the same approach can be extended to eukaryotes as well.

The remainder of this paper is organized as follows. The basic elements of Petri nets are presented in the next section. A following section is used to describe the hierarchical cellular functions of biochemical processes in prokaryotes. Various metabolic reaction mechanisms and the corresponding Petri nets are discussed in section 4. The next section is concerned with the unit models of transportation processes across cell membrane. Different types of operons and their Petri-net models are then described in section 6. In the following section, the Petri-net models of two remaining functional units, i.e., modulon and regulon, are developed in detail. The frameworks of the Petri-net objects are then illustrated in section 8. A systematic procedure for constructing the hierarchical Petri net on the basis of the unit models is presented in the ninth section. The model modification techniques for simulating the effects of gene modification and also the potentially useful information generated with the resulting Petri net are explained with a realistic example in the next section. Finally, to validate the proposed system models, the simulation predictions are compared with experimental data in the literature.

2. Basic Elements in Petri Nets

A formal mathematical description of the ordinary Petri net can be found in Peterson.[30] For the sake of brevity, only a condensed version is provided here. As originally designed, the ordinary Petri net consists of only three types of elements, i.e., places, transitions, and arcs. The state of a discrete-event system is basically reflected with a marking, i.e., a vector of token numbers in all places of the corresponding net. Since only the discrete places are considered in the original Petri net, this vector contains only positive integers and/or zeros. The token movement is realized by enabling and then firing the transitions. A transition is enabled if the token number in every input place is larger than or equal to the weight on the corresponding place-to-transition arc. After firing the transition, tokens are removed from their input places and then introduced into the output places. The number of decreased or increased token(s) in each place is the weight on the arc connecting to the fired transition. It should be noted that the only allowed weight in the ordinary Petri net is 1 and all the transitions are without time delay. To facilitate proper representation of the metabolic phenotype, several special extensions of the ordinary Petri net are adopted in this study.[31,32] Specifically, both discrete and continuous places are allowed and the transitions can be either timed or nontimed in the hybrid Petri nets used in this study. In addition, three different types of place-to-transition arcs are utilized, i.e., the weighted arcs, the

Table 1. Hierarchy in Petri-Net Models for Metabolic Networks

level	components
I	modulon
II	regulon
III	operon
IV	reactions and transport

inhibitor arcs, and the static test arcs. Finally, it should be noted that all transition-to-place arcs are weighted arcs.

3. Hierarchical Structure of Cellular Functions

Recent effort to gain insights of the metabolic phenotype has resulted in the understanding that the cellular functions can be structured into several distinctive units.[5] The classification of functional units is originated from the needs to systematically characterize (i) the enzymatic reaction network, (ii) its control at the genetic level by a common regulatory network, and (iii) the coupling of this regulatory network to the environment through a signal transduction network. It has been well established that an extremely large number of enzyme-catalyzed metabolic reactions can take place in a prokaryotic cell and the needed enzymes are produced in a wide variety of biosynthesis processes. Each enzyme-synthesis process is regulated with a specific control mechanism supported by various *cellular functions*. The primary functional unit of the control mechanism in prokaryotes is the *operon*, which consists of a set of protein molecules (such as the inducer, repressor, mRNA and mRNA polymerase, etc.) and segments of DNA (i.e., the regulator, promoter, operator, structural genes, and terminator sequence). The operons do not function individually in isolation, but rather they are members of a higher-level control network. More specifically, an operon is regulated by a functional unit, the *regulon*, and the regulatory functions of a regulon are often activated by the biosensor signals reflecting specific cell conditions. Furthermore, the control actions of a group of regulons may be coordinated by another function unit, the *modulon*. The modulon responds to physiological states of the cell environment such as the pH value, carbon dioxide and nitrogen concentrations, etc.[2]

Bozinovski et al.[33] proposed a flexible manufacturing system (FMS) metaphor as an alternative means for characterizing the biosynthesis processes. These authors developed the analogies between cellular functions and manufacturing system agents and proposed a unified control framework accordingly for studying both biological and human-made autonomous flexible manufacturing systems. On the basis of the FMS analogy, each biosynthesis process can be viewed as a "recipe" for the production of a specific metabolite. For example, an inducible enzyme is produced if the concentration of a reaction product is low and/or that of the substrate is high. In other cases, the protein synthesis process may be repressed when the required metabolite is produced in sufficient quantity. Consequently, a systematic approach is proposed in the present investigation to construct the Petri-net models to represent these cellular functions. In particular, all cellular functions in prokaryotes are classified into a hierarchy of four different levels according to Table 1. The top-level component is the modulon, which can be considered as a host computer or a human operator in a process plant.

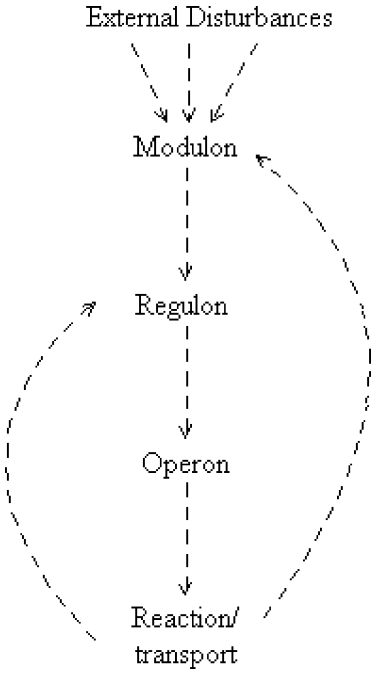

Figure 1. Signal flows among the hierarchical components of a metabolic network.

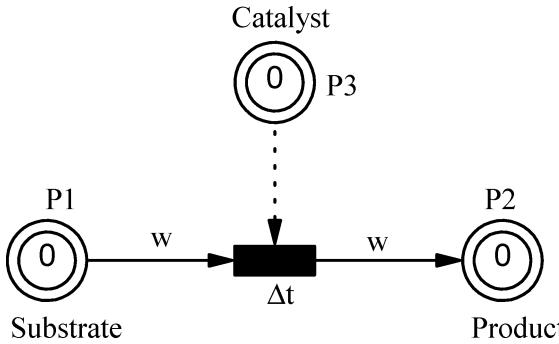

Figure 2. Petri-net representation of an elementary enzyme-catalyzed reaction.

The functions of regulons in the second level can be regarded as the combination of sensors, local controllers, and/or signal transduction systems. The operons are equivalent to the actuators, e.g., hand valves, control valves and switches, etc. Finally, the metabolic reactions and transport mechanisms of metabolites can be considered as the "unit operations" in this plant and classified as level 4 components. A sketch of the signal flows in this hierarchy is presented in Figure 1. The general structures of Petri-net models for all functional units listed in Table 1 are developed in the following sections.

4. Reaction

It has been well established that Petri nets are suitable for modeling chemical reactions.[30] A single-substrate biochemical reaction can be modeled with the net shown in Figure 2. The concentrations of reactant, product, and enzyme are reflected with token numbers in the *continuous* places P1, P2, and P3, respectively. Notice that the reaction step is denoted by a discrete transition with delay time Δt. The weights on its input arc from P1 and output arc to P2 represent, respectively, the amounts of reactant reacted and product produced during the time interval Δt. Specifically, the arc weights can be assigned as $r\Delta t$, where r is the metabolic reaction

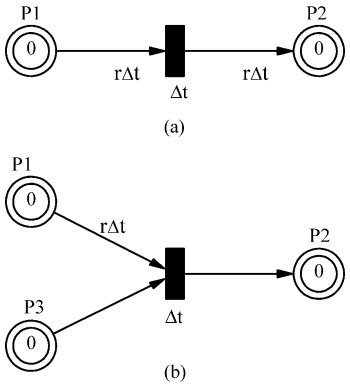

Figure 3. Petri-net models for membrane transport mechanisms: (a) free transport; (b) facilitated or active transport.

rate. It is well recognized that the rates of metabolic reactions can often be determined with the Michaelis–Menten equation:

$$r_1 = \frac{v_1 C_S}{K_1 + C_S} \tag{1}$$

where C_S is the concentration of the substrate, v_1 is the maximum reaction rate, and K_1 is the Michaelis constant. The transition in Figure 2 is enabled whenever the token numbers in its input places are both larger than zero. For bisubstrate reactions, a modified version of eq 1 can be used:[2]

$$r_2 = \frac{v_2 C_{S1} C_{S2}}{(C_{S1} + K_{21})(C_{S2} + K_{22})} \tag{2}$$

where C_{S1} and C_{S2} represent the concentrations of substrates taking part in the reaction, v_2 is the maximum reaction rate, and K_{21} and K_{22} denote the Michaelis reaction constants. In addition, Matsuno et al.[34] modified eq 1 to incorporate the enzyme concentration in the rate expression:

$$r_3 = \frac{v_3 C_C C_S}{K_3 + C_S} \tag{3}$$

where C_C represents the enzyme concentration, v_3 is the maximum reaction rate, and K_3 is the reaction rate constant.

Table 2. Effects of Inhibition on Parameters of the Michaelis–Menten Equation

inhibition mechanisms	v	K
no inhibition	v	K
competitive	v	αK
uncompetitive	v/α'	K/α'
mixed/noncompetitive	v/α'	$\alpha K/\alpha'$

In addition to the elementary enzymatic reactions, the mechanisms of enzyme inhibition should also be considered in constructing Petri-net models. Three types of mechanisms can be identified:[2] (1) competitive, (2) uncompetitive, and (3) noncompetitive. In general, the term *competitive inhibition* is used to represent the scenario when the substrate of an elementary reaction is competing with another metabolite for an enzymatic binding site. This interfering metabolite is referred to as an *inhibitor* in this paper. It can be shown that the maximum reaction rate in the resulting Michaelis–Menten equation remains unchanged, but the Michaelis constant is affected by the inhibitor concentration. On the other hand, the catalytic behavior of an enzyme is altered completely if the inhibition mechanism is *uncompetitive* and thus both the maximum rate and the Michaelis constant must be modified. Finally, the above two mechanisms coexist in the mixed/noncompetitive inhibition mechanism. The corresponding parameters can be obtained by combining the changes adopted in the previous two cases. A summary of the specific effects of inhibition on the parameters of the Michaelis–Menton equation is given in Table 2. In this table,

$$\alpha = 1 + \frac{C_1}{K_I} \tag{4a}$$

$$\alpha' = 1 + \frac{C_1}{K_I^*} \tag{4b}$$

where C_I denotes the inhibitor concentration, and K_I and K_I^* are dissociation constants.

5. Membrane Transport

Molecules can be transported across the cell membrane. Three main categories of molecule transport exist in cells, i.e., *free transport*, *facilitated transport,* and *active transport*.[2] The smaller molecules, e.g., ethanol,

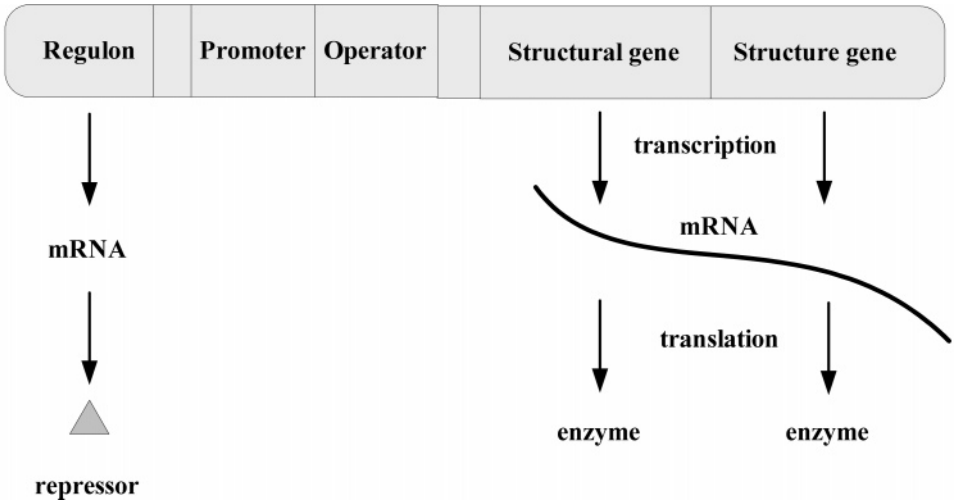

Figure 4. General functions of an operon.

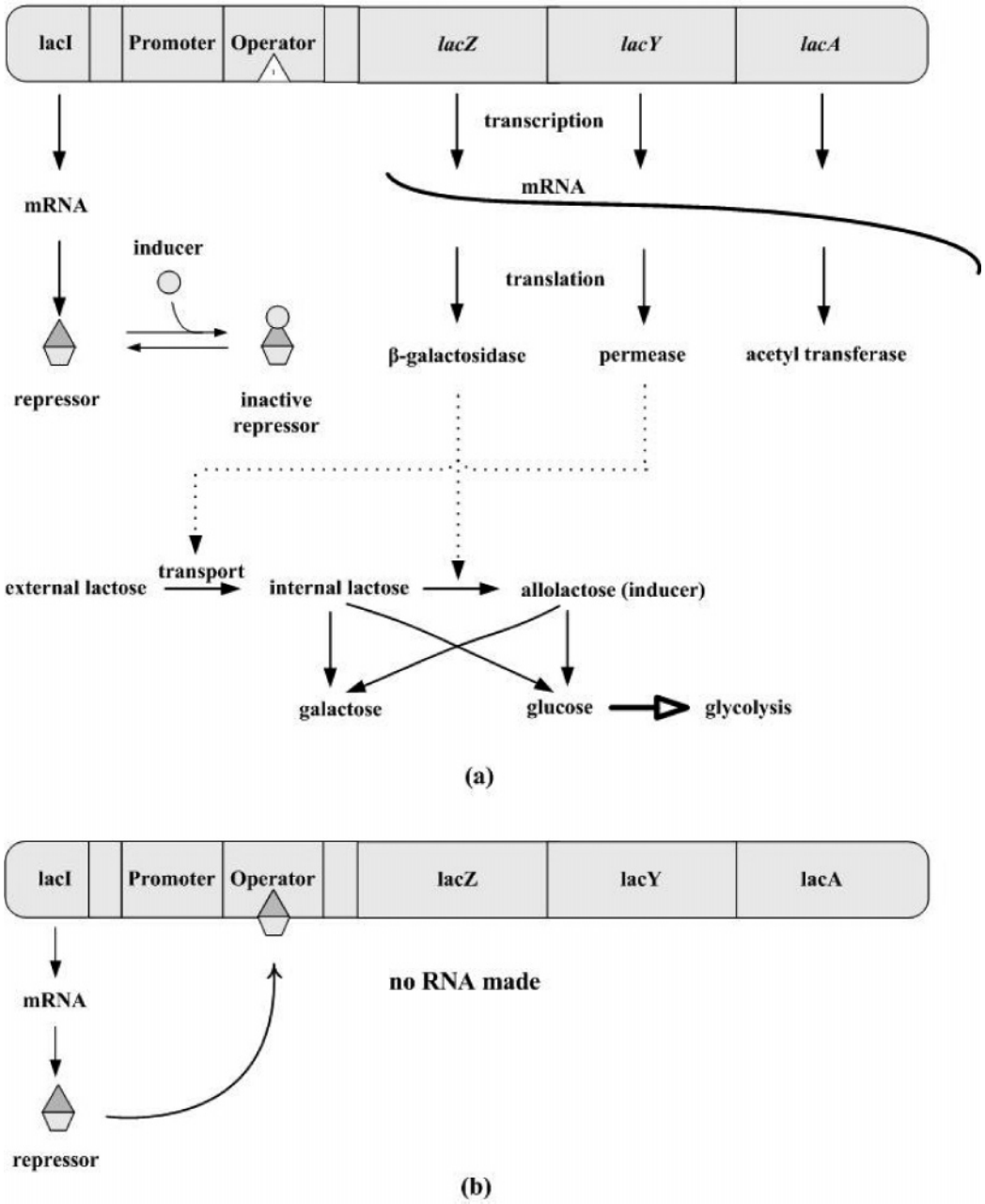

Figure 5. Specific functions of a *lac* operon: (a) in the presence of allolactose; (b) without allolactose.

could easily travel across the cell membrane via simple diffusion mechanisms.[35] The driving force in this case is the concentration gradient. Fick's law can be used to determine the transport rate:

$$r_m = \frac{D_m(C_{CO} - C_{CI})}{d_m} \tag{5}$$

where r_m denotes the rate of molecule transport across the membrane, D_m is diffusivity, C_{CO} and C_{CI} represent the concentrations outside and inside the cell, respectively, and d_m is membrane thickness. On the other hand, many larger compounds (such as proteins, polynucleotides, and polysaccharides) are transported at extremely slow rates by free diffusion because of their very low solubility in the plasma membrane. Carrier molecules can significantly improve the transport rates. This carrier-aided process is referred to as facilitated transport. The active transport mechanism resembles that of facilitated transport. The main difference is that the former can facilitate transportation against the concentration gradient.

The corresponding Petri-net models can be found in Figure 3. The free transport behavior is described in Figure 3a. In this model, the places P1 and P2 represent the concentrations of molecules inside and outside the cell membrane, respectively. The token number of P1 is always higher than that of P2. The arcs connecting transition T with P1 and P2 carry $r_m\Delta t$ as the arc weights. On the other hand, it may be noted from the Figure 3b that an additional place P3 is included to model a facilitated or active transport process. This place (P3) is used to represent the concentration of carrier. The transport rate in this case may be represented as

$$r_f = \frac{D_f C_{P1} C_{P3}}{C_{P1} + C_{P3}} \tag{6}$$

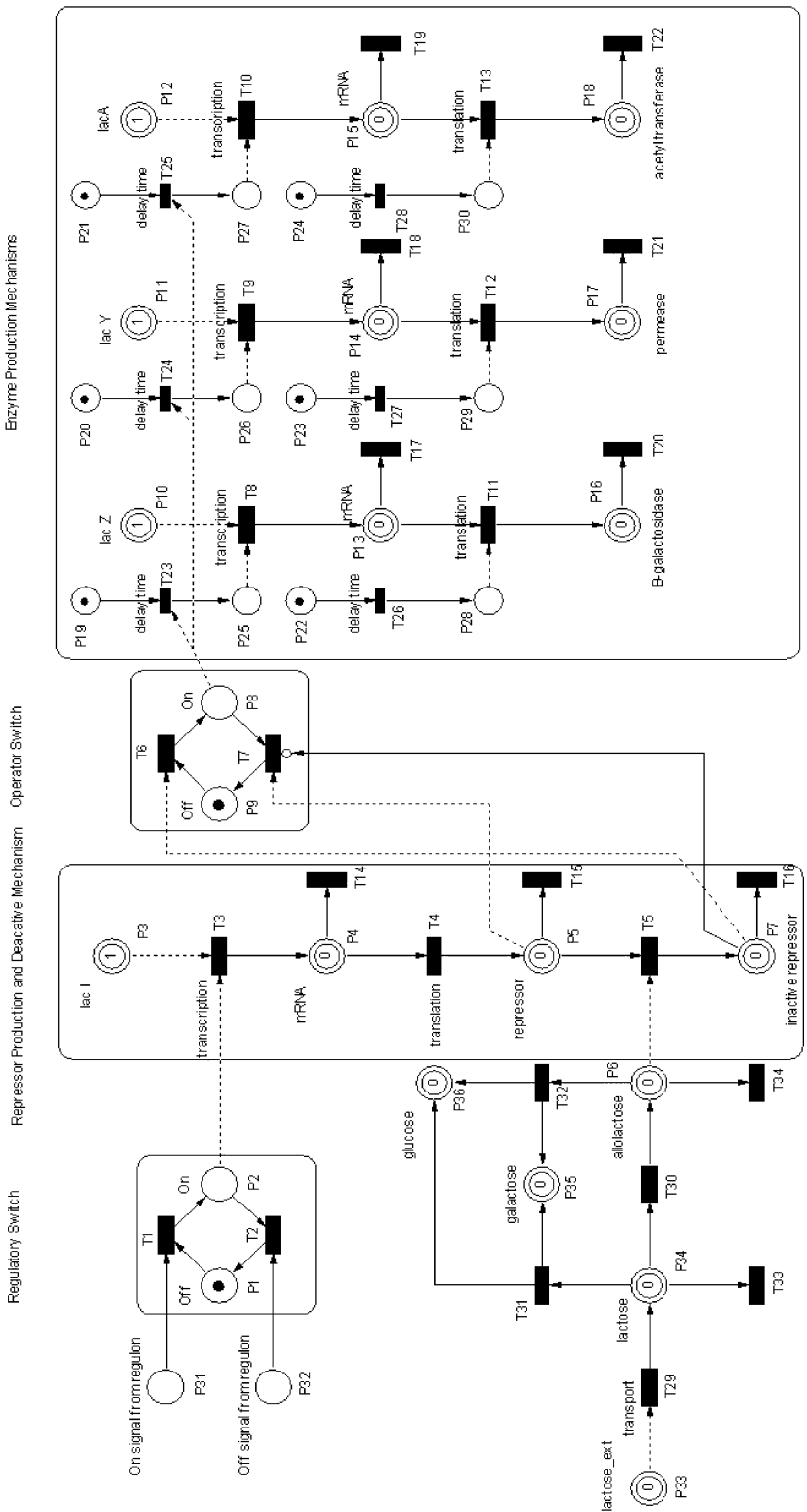

Figure 6. Petri-net model of the inducible operon.

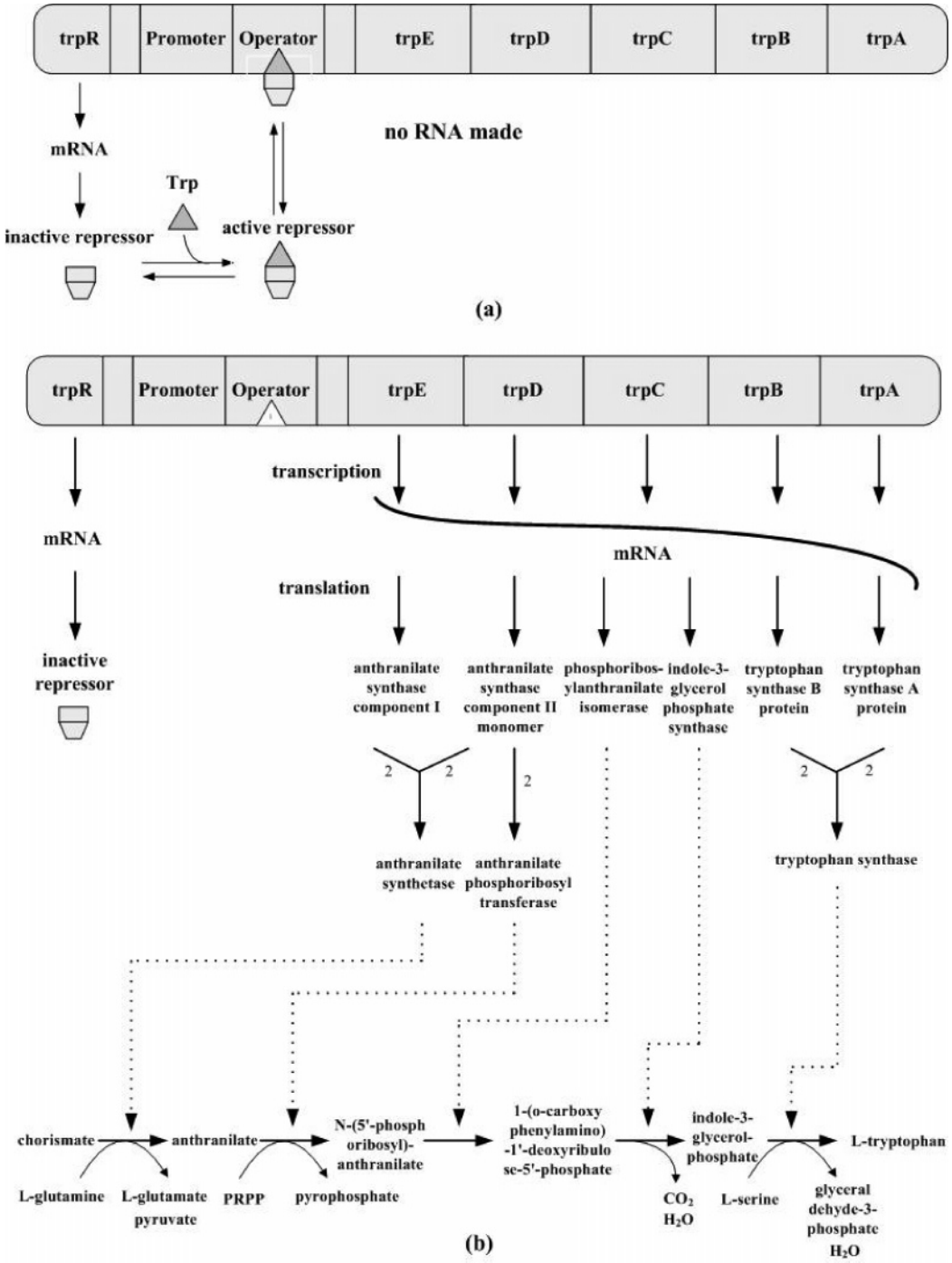

Figure 7. Specific functions of a tryptophan operon: (a) in the presence of tryptophan; (b) without tryptophan.

where D_f is the diffusivity of carrier complex, and C_{P1} and C_{P3} represent the concentrations of biomolecule and carrier molecule, respectively. Again the arc weights in this model can be specified according to the transport rate. Notice that, if the Petri net in Figure 3b is used to describe an active transport process, the token number of P2 is allowed to be higher than that of P1.

6. Operon

The operons are the functional units for enzyme production. As mentioned previously, the cellular functions of each operon are performed with segments of DNA and also protein molecules. The former consist of regulator, promoter, operator, and structural genes. The structural genes encode the required proteins, while the regulatory gene encodes the protein for regulating the expression mechanisms of structural genes. These genes are physically arranged in a sequential array as shown in Figure 4. Various different types of operons have been identified according to their triggering mechanisms, e.g., *inducible, repressible*, and *constitutive*. In an inducible operon, the enzyme is produced only when the inducer/effector molecule are present. More specifically, the inducer molecule binds to the repressor protein and reduces the affinity of the repressor binding to the operator. The *lac* operon is the most celebrated example in this case. The inducer molecule (allolactose) interacts with repressor to form an inactive repressor complex, which has very low affinity toward operator binding. In the absence of inducer molecule, the repressor molecule

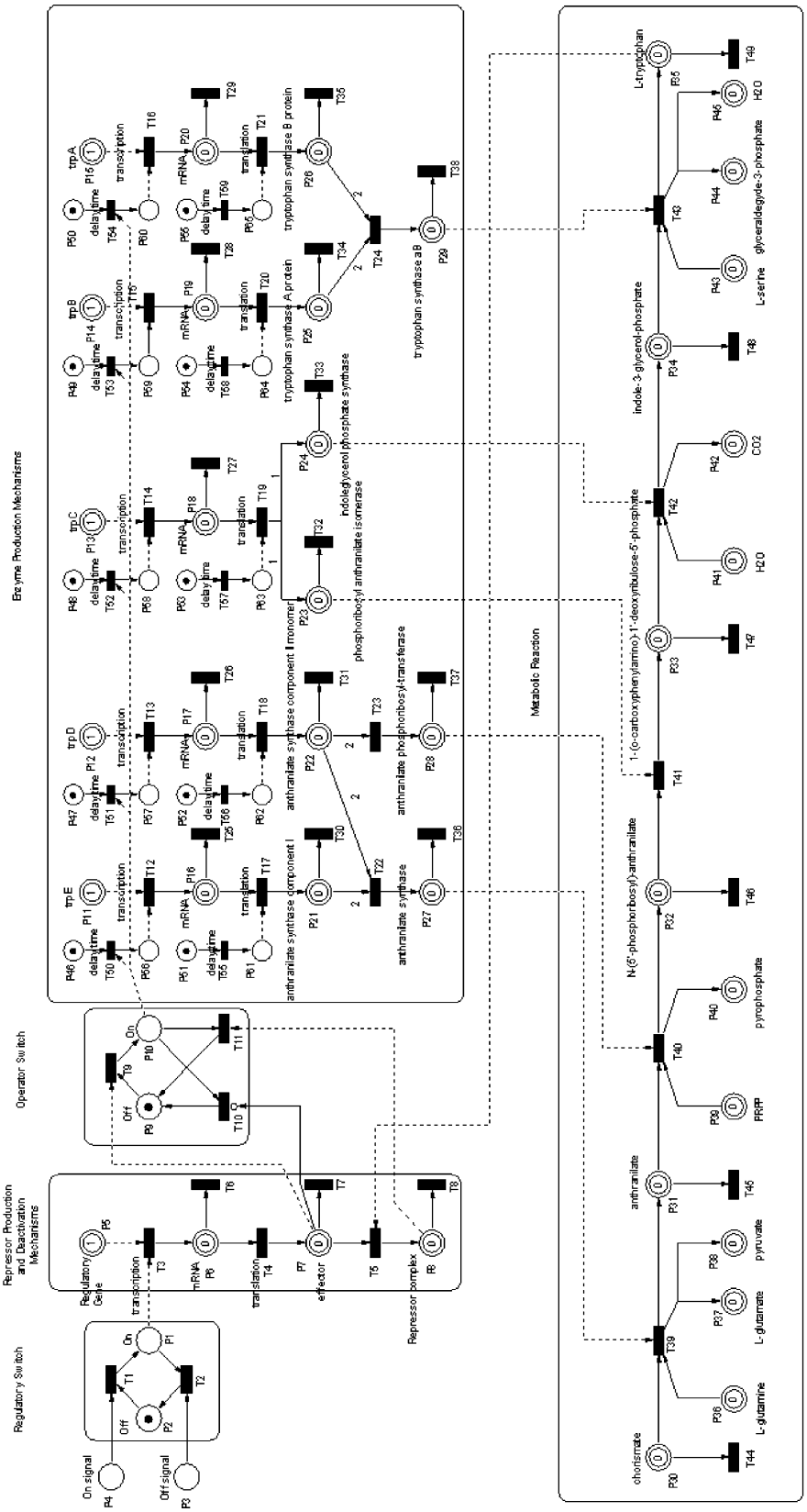

Figure 8. Petri-net model of the repressible operon.

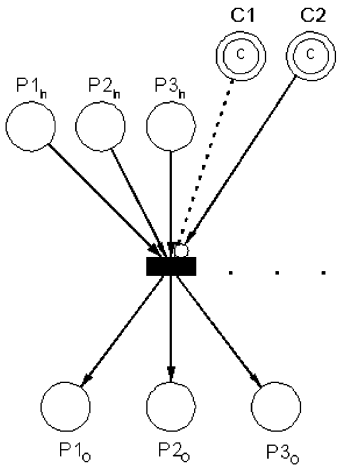

Figure 9. Petri-net model of a regulon.

tends to bind to the operator and shut down the transcription process. On the other hand, the function of co-repressor/effector molecule is just the opposite of that of the inducer in the case of repressible operon. The repressor here does not have binding ability toward the operator. The presence of the co-repressor molecule could promote binding. The trptophan (*trp*) operon is a well-known example of a repressible operon. It always responds to the cell's need to produce tryptophan. However, tryptophan also acts as an effector molecule to enhance repressor binding. As a result, the presence of a significant amount of trytophan tends to shut down the biosynthesis process. Finally, it has been well established that the constitutive enzymes are produced as long as the required raw materials, i.e., the amino acids, are available in the cell environment. Notice that all glycolytic enzymes are constitutive in nature.[36]

A set of generalized Petri nets have been developed to describe all three types of operons mentioned above. Following are the detailed descriptions of these models:

Petri Net Representing Inducible Operons. For illustration convenience, let us consider the specific example of the *lac* operon (see Figure 5). Notice that there are three structural genes in this case, i.e., *lacZ*, *lacY*, and *lacA*. After the regulon triggers the regulatory switch in the *lac* operon, the repressor mRNA and subsequently the repressor are produced. If the inducer is available, then its interaction with the repressor protein should create the inactive repressor complex (Figure 5a) and thus the operator can be freed to activate the structural genes. Consequently, the *lac* operon produces a mRNA with three ribosome binding sites, each of them is transcribed with the activated genes and the end products of the *lac* operon, i.e., β-galactosidase (*lacZ*), permease (*lacY*), and acetyl transferase (*lacA*), can be translated with the corresponding mRNA polymerases. It has been reported that β-galactosidase is involved in converting lactose into glucose, galactose, and allolactose (inducer), while the permease is responsible for transporting lactose from the external environment into the cell.[33] The function of acetyl transferase is still unknown. Finally, it should be noted that the repressor always develops a strong affinity toward the operator without the inducer molecule. If a binding is formed between them, the protein production process will be shut down completely (Figure 5b).

The Petri-net model for the *lac* operon is shown in Figure 6. This model consists of four layers, namely, (1) the regulatory switch, (2) the repressor production and deactivation mechanisms, (3) the operator switch, and (4) the enzyme production mechanisms. The regulatory and operator switches are represented with discrete places while the other two layers are represented with continuous places. All transitions in Figure 6 are discrete. The regulatory switch in the first layer consists of two discrete places (P1 and P2) connected with two discrete transitions (T1 and T2). A token can be introduced in either P1 or P2 to represent the state of the regulatory switch, i.e., off or on. The input places P31 and P32 represent the regulon signals to turn on and off the switch, respectively. The delay times of transitions T1 and T2 are used to reflect the response times of the switch. Notice that the Petri net structure of operator switch is essentially the same as that of the regulatory switch.

The concentrations of regulatory gene (P3), messenger RNA (P4), repressor protein (P5), inducer protein (P6), and inactive repressor (P7) are all described in the second layer of the operon model. Notice that the transcription action (T3) is triggered if gene *lac I* is present and also the regulatory switch is turned on. The mRNA, repressor, and inactive repressor are produced via transcription (T3), translation (T4), and the reaction with inducer allolactose, respectively. On the other hand, they are consumed in the latter two processes mentioned above and also in their respective self-degradation mechanisms. Notice that the presence of inactive repressor prevents the operator switch from being turned off. Furthermore, if its concentration exceeds a certain threshold level and the switch position is "off" (P9) originally, the transition T6 can be fired to move to position "on" (P8). On the other hand, this position can be switched from "on" to "off" if the repressor concentration is above a limiting value and that of inactive repressor is negligibly low at the same time.

The concentrations of structure genes (P10, P11, and P12), messenger RNAs (P13, P14, and P15), and protein products (P16, P17, and P18) are modeled in the fourth layer. More specifically, the places P10−P12 are associated with the structural genes *lacZ*, *lacY*, and *lacA*, respectively, and P16−P18 represent the concentrations of the protein products β-galactosidase, permease, and acetyl transferase, respectively. The self-degradation processes of repressors, mRNAs, and enzymes are characterized with terminal transitions T14−T22. The Petri-net structures used to model the production and consumption processes of the mRNAs are in essence the same as those for the repressor mRNA. Finally, notice that the delay times of transitions T23−T25 represent the times required to produce the messenger RNAs, and those assigned to T11−T13 are used to reflect the times required to produce β-galactosidase, permease, and acetyl transferase, respectively.

The rates of decomposition and self-degradation can be specified with the weights on the corresponding place-to-transition arcs. Lee and Bailey[37,38] suggested that these reaction rates could be determined according to

$$r_d = K_d C_X \tag{7}$$

where K_d represents the reaction constant and C_X denotes the concentration of protein molecules, i.e., the token number of the input place. On the other hand, the generation rate of a particular protein in this operon

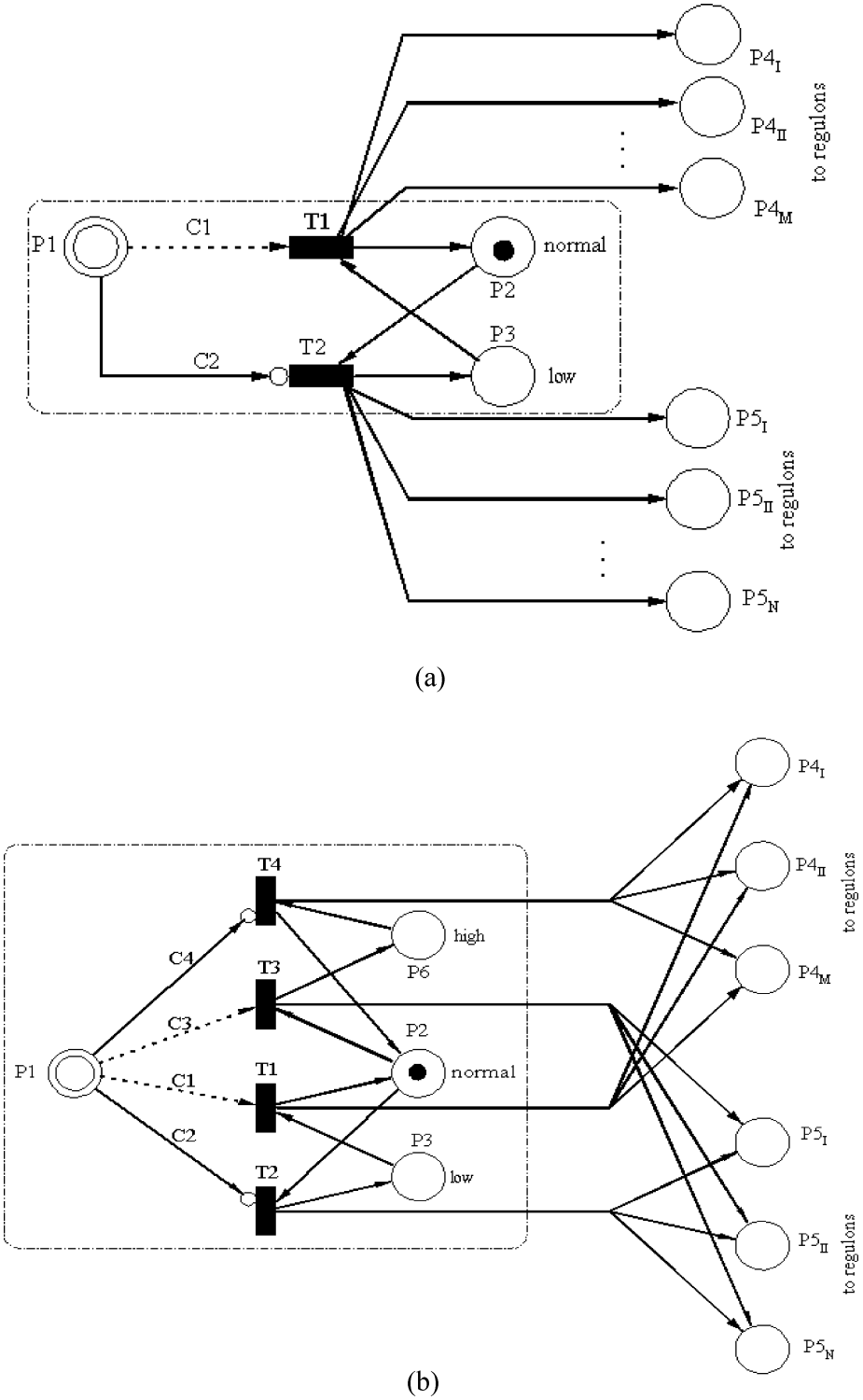

Figure 10. Petri-net models of modulons: (a) for describing the impacts of lower-than-normal process parameters; (b) for describing the impacts of abnormal process parameters in general.

is specified with the weight on the corresponding transition-to-place arc. In general, this rate should be the same as the weight on the place-to-transition arc connecting to its input transition. For example, in Figure 6, the weight associated with the arc connecting transition T3 and place P4 can be regarded as the generation rate of repressor mRNA and C_X in this case should be the concentration of regulatory gene.

Petri Net Representing Repressible Operons. The *trp* operon is considered here as an example for illustrating the Petri-net structure for repressible operons (see Figure 7). This operon has five structural genes: *trpA*, *trpB, trpC, trpD*, and *trpE*. The genes *trpE* and *trpD* are needed in the production of an enzyme anthranilate synthetase. On the other hand, the gene *trpC* is responsible for encoding indole-3-glycerol phosphate synthase and phosphoribosylanthranilate isomerase, along with *trpA* and *trpB*, is the precursor for synthesizing the end product tryptophan. It may also be noted that, in the *trp* operon, tryptophan itself acts as an effector called the *co-repressor*. An increase in its concentration triggers the reaction with repressor pro-

tein to form the repressor dimer. The dimer enhances the binding of repressor toward the operator and halts the protein synthesis process. The Petri-net model for this repressible operon is given in Figure 8. Notice that it is very similar to the Petri net for describing the inducible operon (Figure 6). The major differences between the two are concerned with the operator switch and functional activities of repressor production and deactivation mechanisms (the second layer) and enzyme production mechanisms (the fourth layers). For the sake of brevity, the detailed explanation of net structure is not repeated here.

Petri Net Representing Constitutive Operons. As mentioned earlier, a constitutive operon produces enzyme(s) as long as the required raw materials are available. The PN model for such an operon can thus be constructed simply according to the first and fourth layers of the Petri net representing an inducible operon.

7. Regulon and Modulon

The functional molecules in a regulon play the roles of sensors, local controllers, and signal transducers in the cell metabolism. The regulon reacts to signals from a modulon or from the sensor molecules. A general model of regulon is given in Figure 9. Notice that the regulon is essentially a multi-input and multi-output component. The inputs are basically sensor (C1, C2, ...) or modulon signals ($P1_{in}$, $P2_{in}$, ...). The outputs can be used as the activation/deactivation signals to operons or as inputs to other regulons. Thus, a group of regulon models can be arranged in parallel or in series as required.

Finally, a modulon reacts to changes in the conditions of cell environment, e.g., oxygen concentration, nutrition content, temperature, etc., with control signals to various regulons. A generalized Petri-net model can be developed to characterize the modulon behaviors. Let us first consider the Petri net given in Figure 10a. This model consists of a continuous place (P1) and two discrete places (P2 and P3) connected with two discrete transitions (T1 and T2). Here, P1 is used to reflect a particular environment condition, e.g., the oxygen concentration. The modulon function is activated or deactivated on the basis of the token number in P1. On the other hand, P2 and P3 represent, respectively, two different qualitative concentration ranges, i.e., "normal" and "low". The place P1 is connected to transition T1 with a test arc and to another transition T2 with an inhibitor arc. The arc weights C1 and C2 (C1 ≥ C2) denote, respectively, the upper and lower threshold limits between the two qualitative ranges. The transition T1 is connected to P2 and also $P4_1-P4_M$ with normal arcs. The latter places are used to represent the activation/deactivation signals of a set of different regulons. Similarly, the transition T2 is connected to P3 and also to the places $P5_1-P5_N$ denoting the signals for another set of regulons. Finally, to ensure that the states associated with places P2 and P3 are mutually exclusive, the former is connected to T2 and the latter T1.

Notice that the Petri net in Figure 10a can only be used to describe the impacts of lower-than-normal process parameters. Its mirror image can be easily constructed to model the adverse effects caused by the opposite, i.e., higher-than-normal, environment conditions. These two nets can then be combined to form a more complete version of the modulon model (see Figure 10b). In this model, the place P6 is used to reflect the higher-than-normal concentration range and the arc weights C3 and C4 (C3 ≥ C4) denote the threshold limits between the concentration ranges "high" and "normal" respectively.

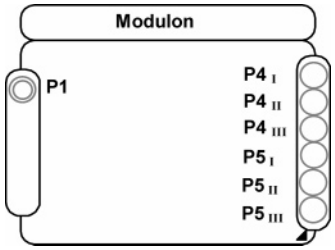

Figure 11. Object frame of the modulon model.

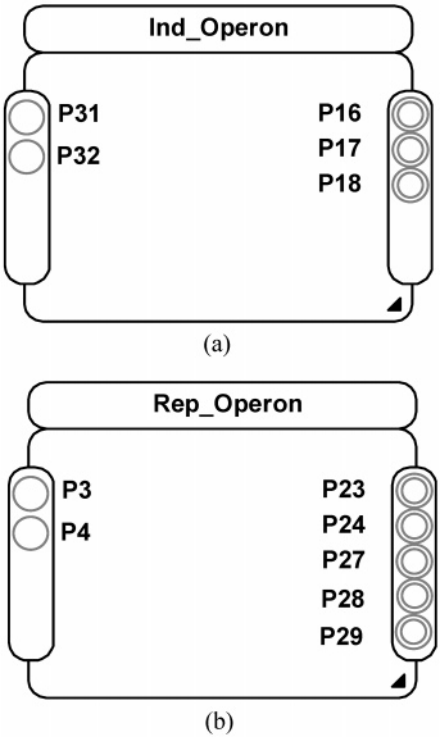

Figure 12. Object frames of the Petri-net models of (a) inducible operon and (b) repressible operon.

8. Petri-Net Objects

The unit models developed in the earlier sections can be packaged as objects to enhance the readability of the Petri nets. For illustration purpose, let us first consider the modulon model in Figure 10a as an example. Since it is only necessary to consider the inputs and outputs of each unit model in building the system model, the corresponding connecting ports should be provided on the object frame of modulon (see Figure 11). It may be noted that the places representing the intrinsic unit states, i.e., P2 and P3, are not shown on the frame. Let us next consider the Petri-net model of the inducible operon in Figure 6. Although this Petri net has four layers with many places and transitions, the connecting ports with other functional units are places representing (i) regulon signals (P21 and P22), (ii) the concentration of β-galactosidae (P16), and (iii) the concentration of permease (P17). Accordingly the operon model can be packaged and its object frame is given in Figure 12a. Finally, the Petri-net model of repressible operons can

Table 3. Construction Procedure of System Model

step 1	depict the primary and auxiliary reaction/transport networks
step 2	construct the signal flow configuration in the gene regulatory network involving modulon, regulon, and operon
step 3	select the appropriate unit models
step 4	assemble the unit models according to the reaction/transport networks and signal flow configuration obtained in steps 1 and 2

be packaged in a similar fashion. The resulting object frame is shown in Figure 12b.

9. Model Construction Procedure

The integrated system model can be constructed by connecting the Petri-net objects. A systematic model-building procedure has been developed in this study (Table 3). Let us consider the reaction/transport network presented in Figure 13 as an example. This artificial system was configured to imitate the typical metabolic pathways of glucose, including basically the transportation process across cell membrane and the following anabolism reactions. For illustration convenience, the reaction kinetics and gene regulation mechanisms are chosen to make the following discussions easy to comprehend. The reactions r1−r12 represent the primary reaction network where reactant A is converted to product F. The intermediates (B to E and G to J) are formed and consumed in these reactions. It is assumed that only A^1 and F can be transported across the cell membrane. The former is enabled in a facilitated transport process Tr1 and the latter a free transport process Tr2. The metabolites K, X, and Y are produced and/or consumed in the auxiliary reactions r13−r16. Notice that X and Y are also involved in the primary reactions r1, r3, r4, and r5. The symbols c1−c16 are used to represent the enzymes for the corresponding reactions. It is assumed that c12 is inducible and c6 and c15 are repressible, while all other enzymes are constitutive. In addition, we assumed that

•Enzyme c15 is produced only when the reactant A is lower than a certain threshold value.

•The resulting increase in the concentration of K activates the inducible operon for c12.

•The inducible operon produces two enzymes, i.e., cr1 and c12. The enzyme cr1 supports the transport of A^1 while c12 is the catalyst of reaction r12.

•The production of c6 is suppressed when the concentration of intermediate C builds up.

Let us now try to follow the construction steps listed in Table 3 to build a system model:

Step 1. The primary and auxiliary reaction/transport networks are presented in Figure 13.

Step 2. The signal flow diagram of the above reaction system can be found in Figure 14. It may be noted that, in the regulatory and signal transduction networks, there are one modulon, four regulons, and 16 operons. The labels *Ope_r1* and *Ope_r2* denote two different repressible operons; *Ope_in* represents an inducible one; *Ope_c1* to *Ope_c13* are 13 different constitutive operons. Variations in the environment conditions are sensed by the modulon. The lower and upper threshold values of temperature in the cell environment have been assumed to be 35 and 50 °C, respectively, while the threshold values of pH are 5 and 9. Signals reflecting pH and temperature are directed to the regulon *Reg_1* only, and on the other hand, information about nutrient is transmitted to every regulon. *Reg_1* switches on all constitutive operons as soon as nutrient availability is confirmed by the modulon. *Reg_4* activates *Ope_r1* after receiving the nutrient availability information from modulon and deactivates the same operon when the concentration of C is above 1 mM. *Reg_2* activates (or deactivates) the repressible operon *Ope_r2* when the concentration of A

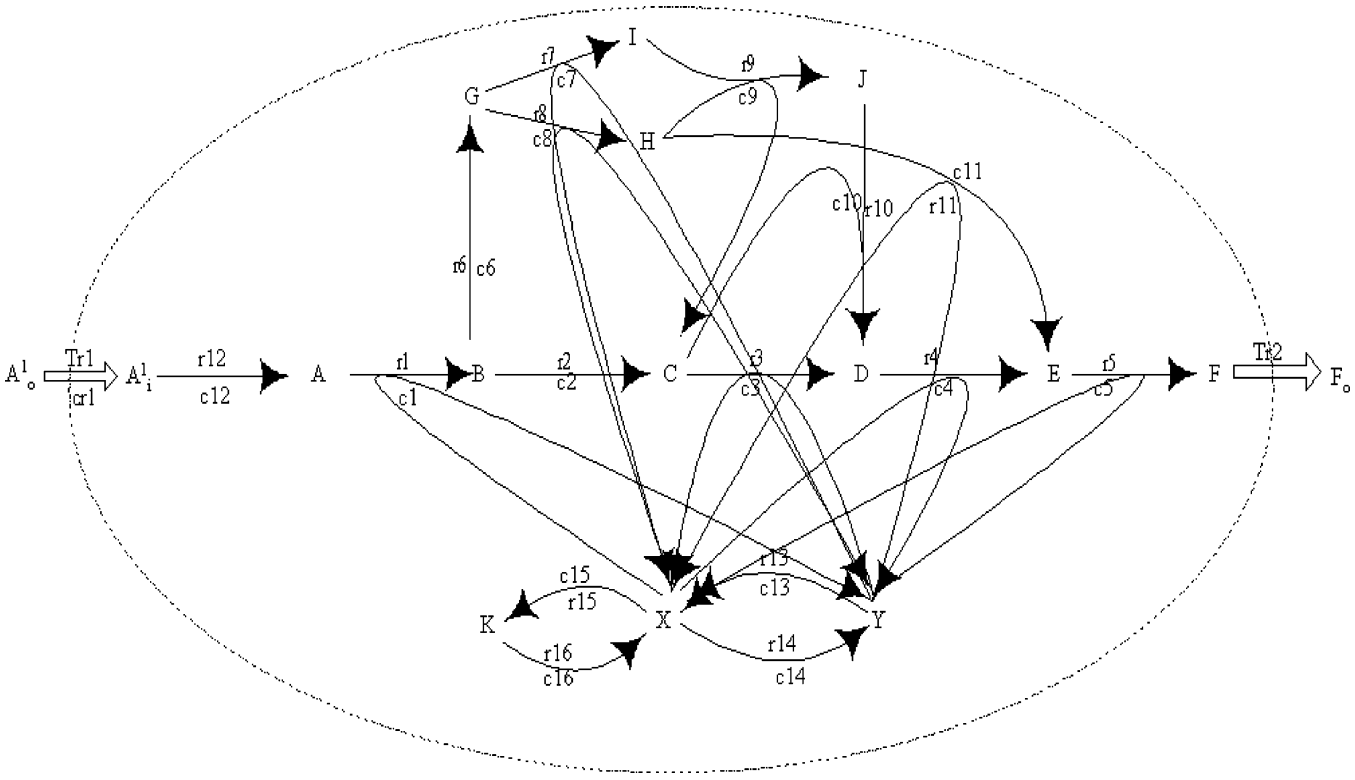

Figure 13. Typical reaction/transport network.

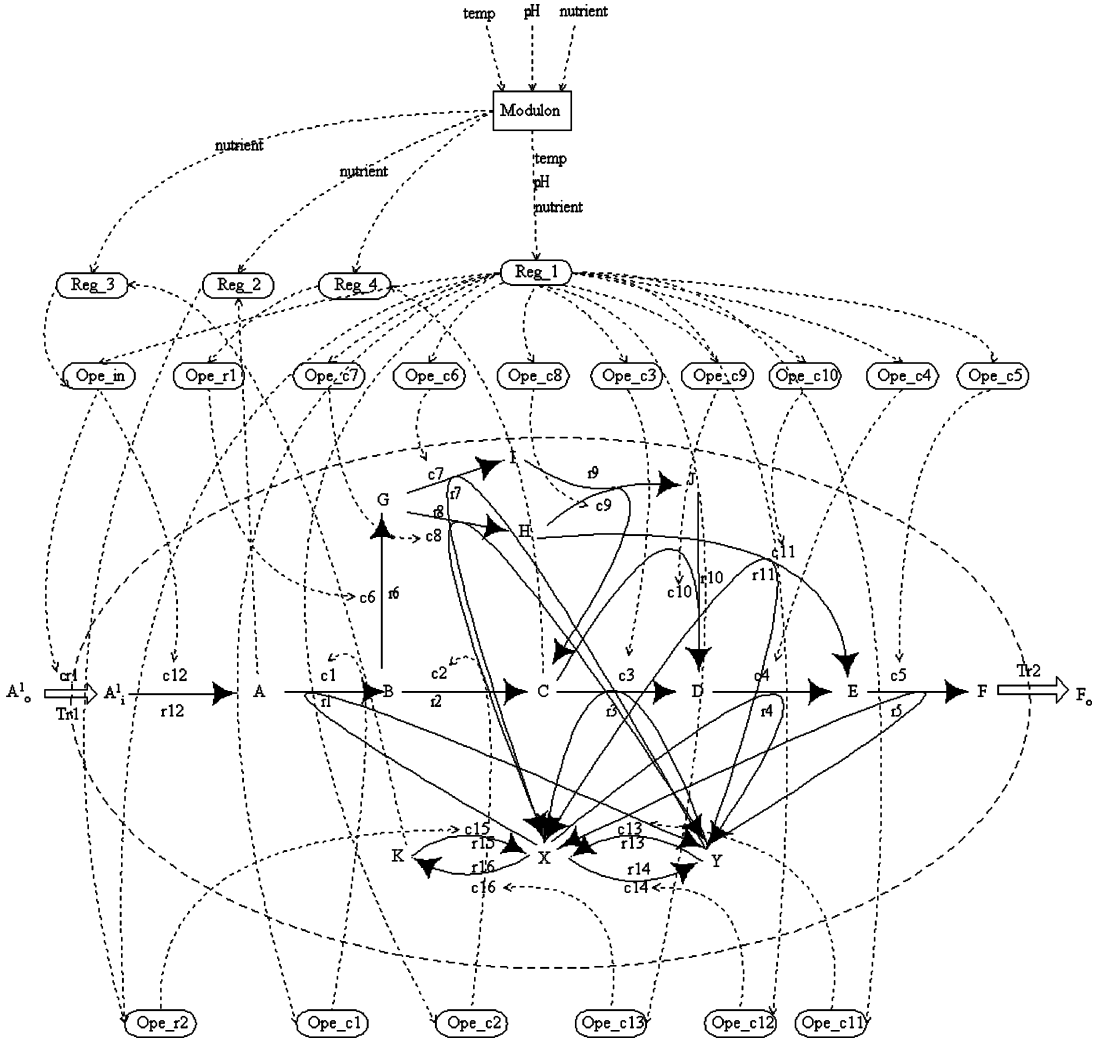

Figure 14. Signal flow diagram for the reaction/transport scheme given in Figure 13.

decreases to a level less than 15 mM (or increases to a level above 16 mM). The subsequent production of K could cause *Reg_3* to trigger the inducible operon *Ope_in* as long as its concentration is above zero.

Step 3. Appropriate unit models have been selected for the system given in Figure 14. The modulon models developed previously have been adopted in this example to describe the effects of nutrients (Figure 10a) and the effects of temperature and PH (Figure 10b). The unit models given in Figures 6 and 8 have been chosen to represent the inducible and repressible operons, respectively. As suggested previously, the first and fourth layers of the unit model of an inducible operon can be used to represent the constitutive operons. This approach has been followed to describe *Ope_c1*−*Ope_c13*. Table 4 gives the rate equations used in the operon models. Both primary and auxiliary reactions are described on the basis of the model structure given in Figure 1. The transportation processes of A^1 and F are represented with the unit models presented in Figure 3. The rate equations for the reaction and transport processes are listed in Table 5.

Step 4. The system model can be constructed by connecting the Petri-net objects of unit models according to the reaction/transport networks in step 1 and signal flow configuration in step 2.

Simulation studies can be performed according to the above hierarchical Petri net to generate useful information. Before executing the model, additional initial conditions should be specified:

Table 4. Rate Equation Used in Protein Synthesis

rate equation	K	remarks
$r = KC_S$	1	production of mRNA
	0.25	self-degradation of mRNA
	0.85	production of repressor/activator
	0.25	self-degradation of repressor/activator
	0.85	production of enzyme
	0.75	self-degradation of enzyme
	0.1	self-degradation of inactive repressor/active effector
$r = \frac{KC_{S1}C_{S2}}{(1 + C_{S1})(1 + C_{S2})}$	1	production of inactive repressor/ active effector

•The initial concentration of reactant A is 20 mM and those of X and Yare both 5 mM. The concentrations of all other metabolites are zero initially.

•Initially, the state of modulon is "normal". The initial temperature and pH of the cell environment are maintained at 35 °C and 7, respectively. Nutrient concentration is assumed to be maintained at 1 mM throughout the entire simulation period.

•All places in the regulons are empty initially.

•All places in the operons are empty except those representing regulatory gene, inducer/activator protein, and structural genes. Their concentrations are maintained at 1 mM throughout the simulation period.

The simulation runs in this work were implemented with a commercial software, Visual Object Net++.[32] The

Table 5. Rate Equations of Reaction Transitions in System Model

reaction	reactant	product	catalyst	rate expression
r1	A,X	B, Y	C1	$\frac{C_{C1}C_A C_X}{(C_A+1)(C_X+1)}$
r2	B	C	C2	$\frac{C_{C2}C_B}{(C_B+1)}$
r3	C,Y	D	C3	$\frac{C_{C3}C_C C_Y}{(C_C+1)(C_Y+1)}$
r4	D,X	E	C4	$\frac{C_{C4}C_D C_X}{(C_D+1)(C_X+1)}$
r5	E,Y	F	C5	$\frac{C_{C5}C_B C_Y}{(C_B+1)(C_Y+1)}$
r6	B	G	C6	$\frac{C_{C6}C_B}{(C_B+1)}$
r7	G,X	I	C7	$\frac{C_{C7}C_G C_X}{(C_G+1)(C_X+1)}$
r8	G,Y	H	C8	$\frac{C_{C8}C_G C_Y}{(C_G+1)(C_Y+1)}$
r9	I,H	J,C	C9	$\frac{C_{C9}C_H C_Y}{(C_H+1)(C_I+1)}$
r10	C,J	D	C10	$\frac{C_{C10}C_C C_J}{(C_C+1)(C_J+1)}$
r11	H,Y	E	C11	$\frac{C_{C11}C_H C_Y}{(C_H+1)(C_Y+1)}$
r12	A^1	A	C12	$\frac{C_{C12}C_A}{C_A+1}$
r13	Y	X	C13	$\frac{C_{C13}C_Y}{C_Y+1}$
r14	X	Y	C14	$\frac{C_{C14}C_X}{C_X+1}$
r15	X	K	C15	$\frac{C_{C15}C_X}{C_X+1}$
r16	K	X	C16	$\frac{C_{C16}C_X}{C_X+1}$
Tr1	$A^1{}_o$	A^1	Cr1	$\frac{C_{\alpha 1}C_{A'_o}}{C_{A'_o}+1}$
Tr2	F	F_o		C_F

simulation results are given in Figure 15. It may be noted that the concentration of reactant A reduces to 15 mM from its initial value of 20 mM within a few seconds and fluctuates around the same value for rest of the process time. This is due to the fact that the repressible operon for c15 (*Ope_r2*) is switched on when the concentration of A reduces to a level less than 15 mM. Consequently, the triggered reaction r15 causes an increase in the concentration of K. This increase activates the inducible operon (*Ope_in*) later and thus the catalysts cr1 and c12 can be produced. As mentioned before, the catalyst cr1 is responsible for the transportation of A^1 and c12 is for the conversion of A^1 to A. As a result, reactant A is consumed and then produced again periodically as shown in Figure 15a. The moderate fluctuation of C_A around 15 mM is due to the conditions assigned for the inducible operon *Ope_in* and repressible operon *Ope_r2*. The concentration of intermediate B increases to 0.5 mM and stays around the same value for the rest of the reaction time. The marginal fluctuation of C_B is due to the fluctuation of C_A. This effect can also be observed in the concentration of other intermediate metabolites, i.e., C_C-C_E and C_G-C_J. Notice that C_F increases monotonically with reaction time as the transport rate of F is relatively low. The concentration of auxiliary metabolite X reduces initially from 5 mM within a few seconds and then fluctuates around 2 mM for the rest of the reaction period. The initial reduction in C_X is because X is involved in reaction r1 through

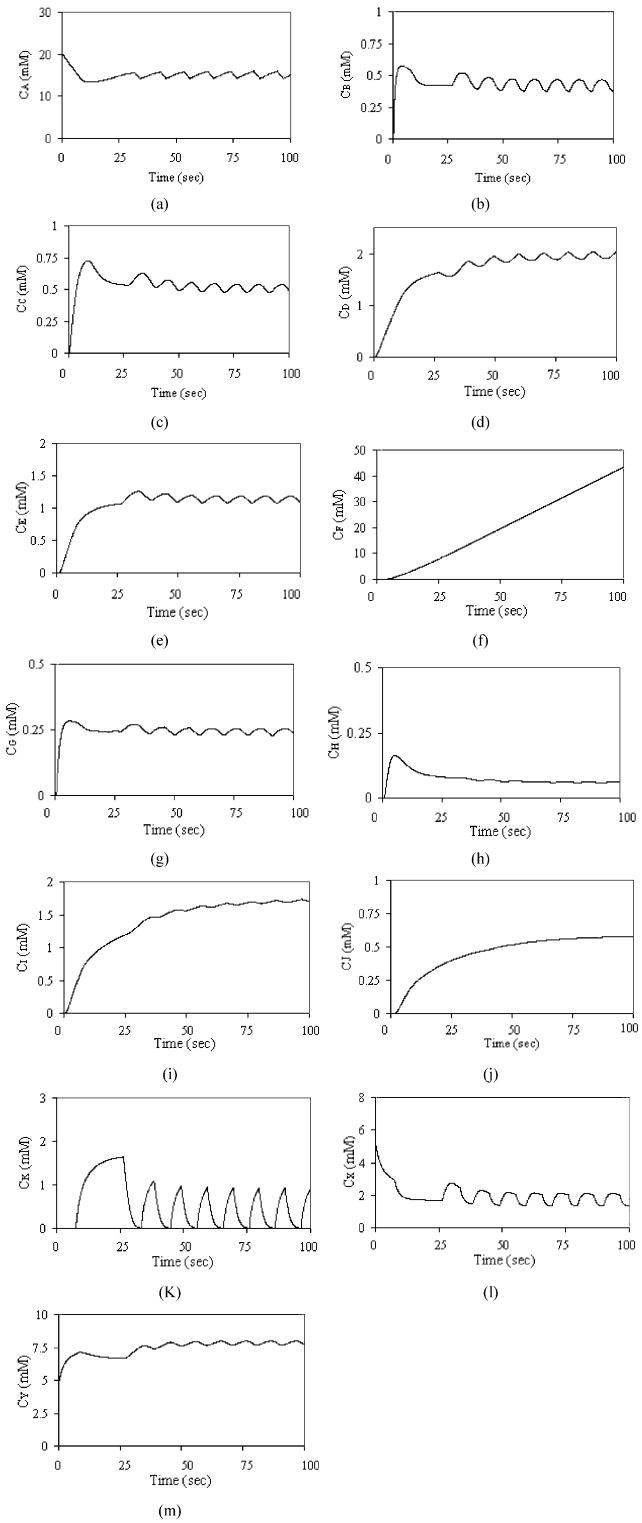

Figure 15. Simulation results obtained with the system model of the metabolic network given in Figure 14 under normal operation.

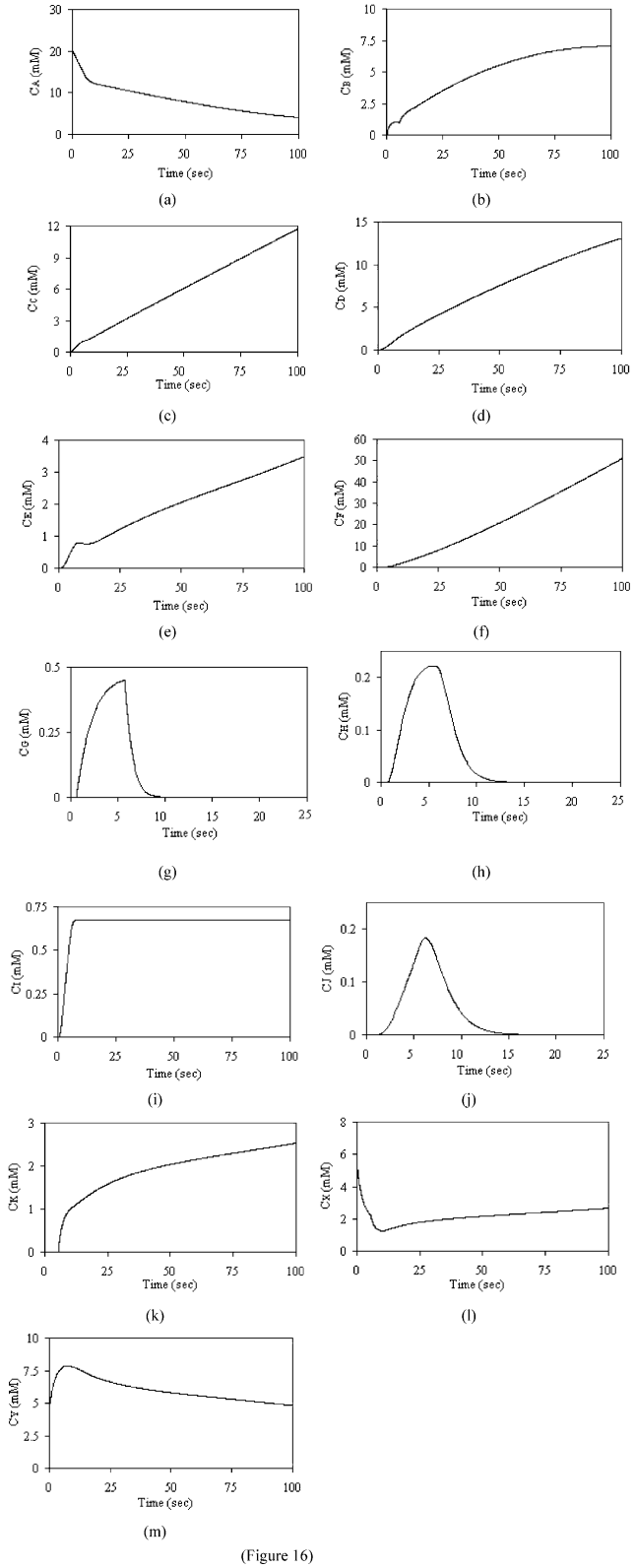

(Figure 16)

Figure 16. Simulation results obtained with the system model of the metabolic network given in Figure 14. Case 1: Reaction rate of r1 is increased via gene modification.

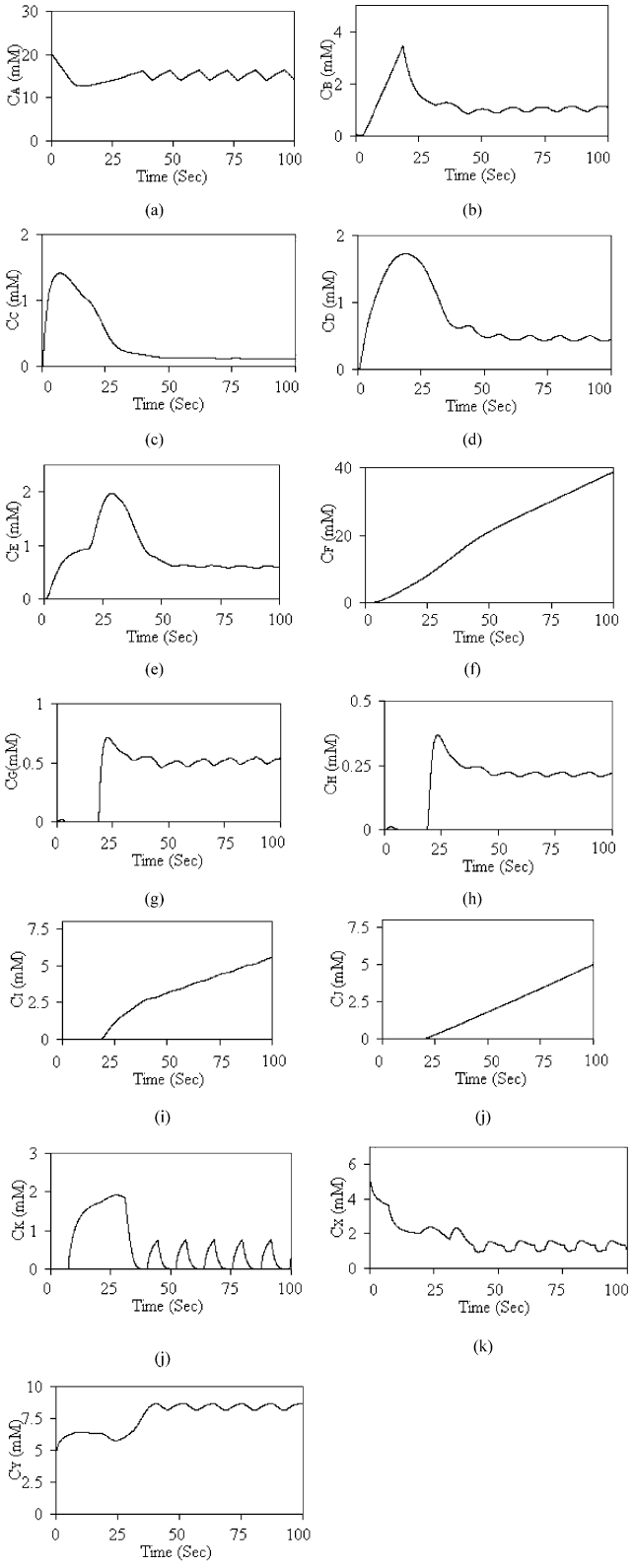

Figure 17. Simulation results obtained with the system model of the metabolic network given in Figure 15. Case 2: Reaction rate of r2 is slowed due to feedback inhibition.

which the metabolite flux is higher than other competing reactions. This effect is also reflected in C_Y. Finally notice that the metabolite K forms and decomposes intermittently. This phenomenon may be explained by the fact that catalyst c15 (which facilitates reaction r15) is produced whenever the concentration of reactant A reduces to a level below 15 mM and the production of c15 is halted when C_A reaches 16 mM.

10. Predicting the Effects of Gene Modification

As mentioned before, it is desirable to produce credible predictions of the effects of gene modification in

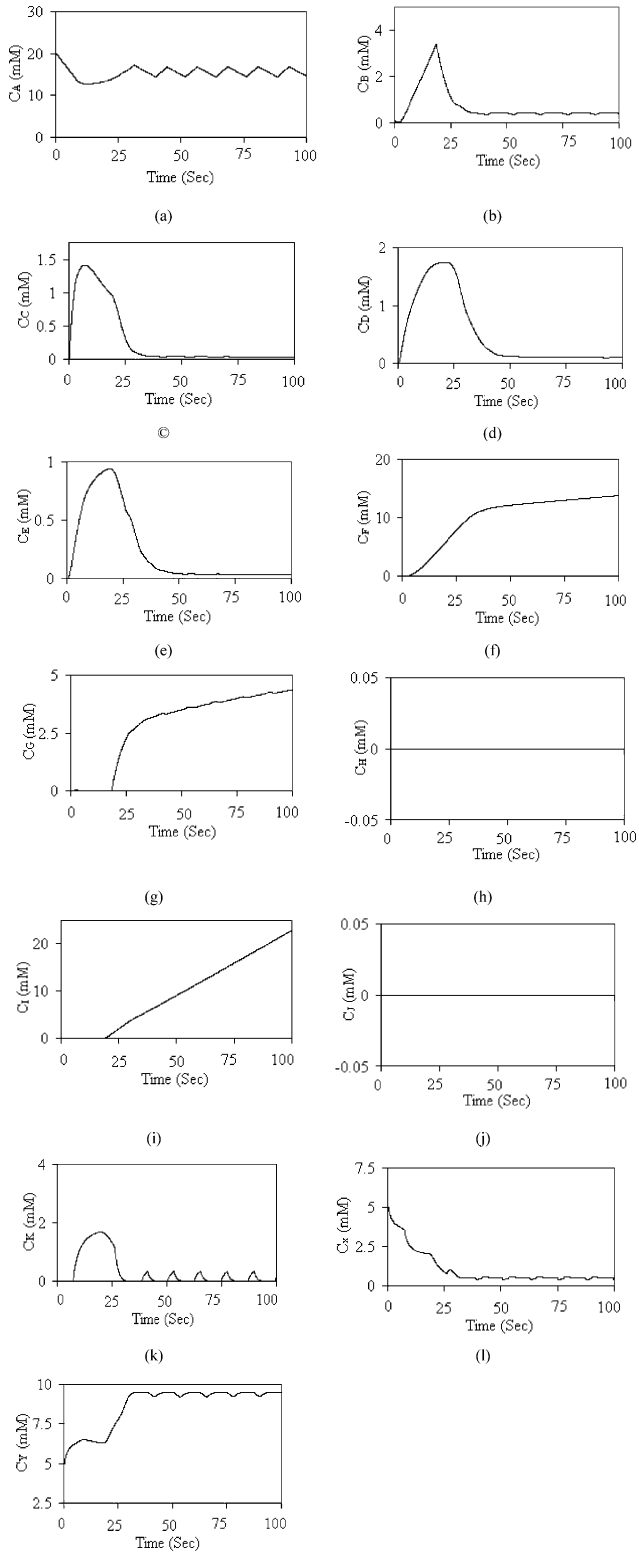

Figure 18. Simulation results of the system model in Figure 15. Case 2: Flux is re-routed through an alternative pathway in a system with feedback inhibition on r2.

many metabolic engineering studies. To demonstrate the descriptive power of the proposed model in such applications, two additional case studies have been carried out on the basis of the example system described above:

Case 1: Reaction Rate of r1 Is Increased via Gene Modification. Let us assume that the reaction rate of r1 in the original system can be improved

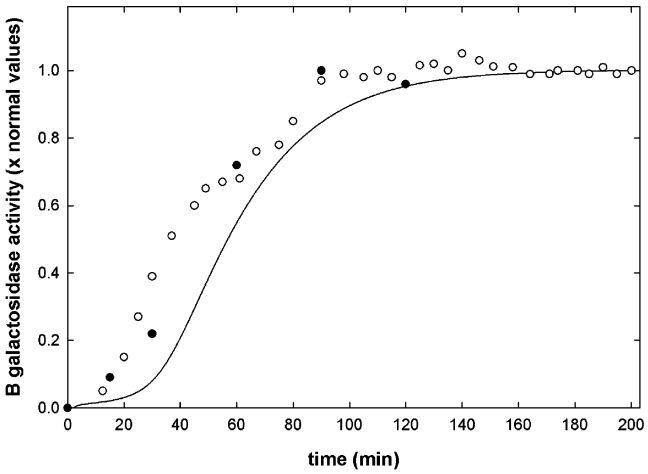

Figure 19. Simulation results of Petri-net model compared with experimental data from Knorre[41] (○) and Pestka et al.[42] (●).

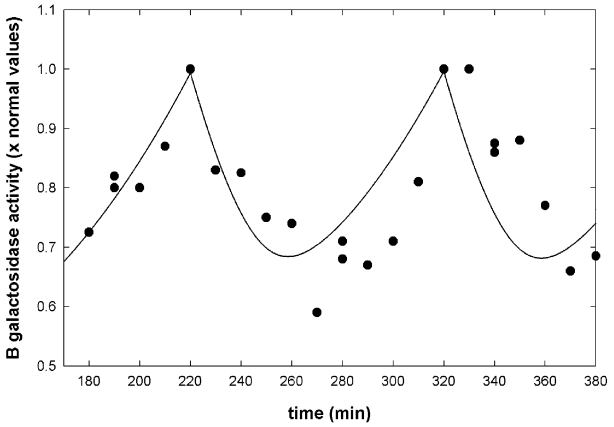

Figure 20. Simulation results of Petri-net model compared with experimental data from Goodwin[43] (●).

through gene modification. Its direct effect can be modeled by adjusting the rate constant for enzyme production in *Ope_c1*. In particular, the original value of 0.85 used in the fifth row of Table 4 has been changed to 1.25. The increased enzyme concentration could enhance the rate of r1 since the rate equation in this case is taken from the first row of Table 5. The simulation results are given in Figure 16. Notice that the concentration of reactant A now decreases monotonically without fluctuation. The rate of concentration decrease is large shortly after reactions begin and then gradually reduces to a lower level. The sharp decrease of C_A in the initial stage may be attributed to the facts that the inducible operon *Ope_in* and repressible operon *Ope_r2* are off initially and are both activated later when C_A reduces to below 15 mM. In other words, the sharp decrease of C_A should occur before the production of inducible catalyst c12. On the other hand, the more gradual decrease of C_A later reveals that the rate of decomposition (reaction r1) is higher than the rate of production (reaction r12) as the rate of r1 is improved via gene modification.

The concentrations of intermediate metabolites B−F increase with reaction time. This is again due to the significant increase in the rate of r1. Another interesting observation is the behavior of C_G. Notice that after attaining a certain concentration, the metabolite G depleted completely. This is because the production of

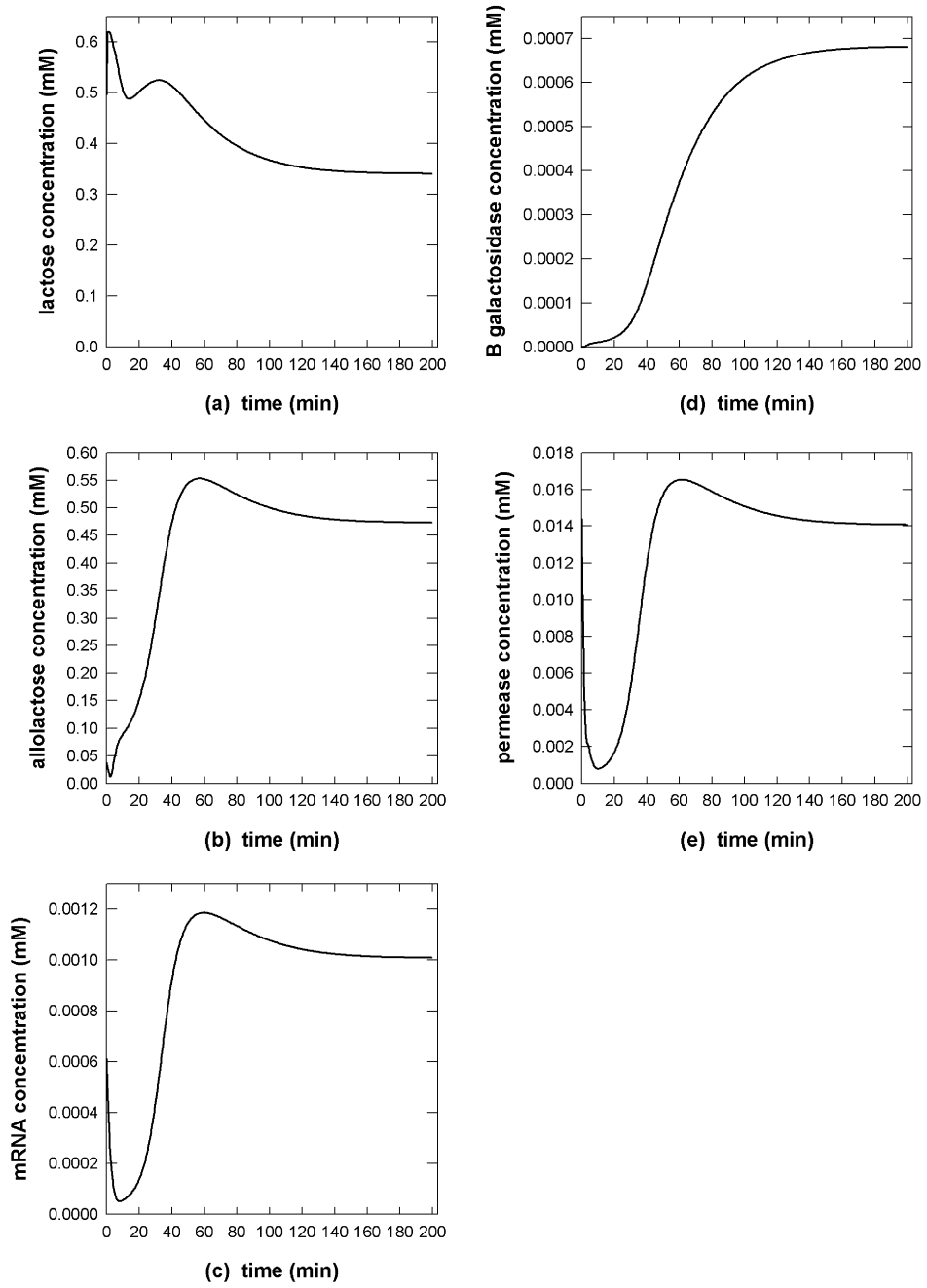

Figure 21. Simulation results obtained with Petri-net model at an initial lactose concentration of 0.08 mM: (a) internal lactose, (b) allalactose, (c) mRNAz, (d) β-galactosidase, and (e) permease.

enzyme c6 is suppressed when the concentration of C is above 1 mM (see Figure 16c). It should be noted that C_C in the previous case study is kept below 1 mM throughout the entire reaction period (see Figure 15c). Notice also that the behavior of C_H is similar to that of C_G. This can be explained by the fact that the metabolite H is produced as long as C_G is above zero and consumed completely after C_G becomes zero.

On the other hand, it can be observed that C_I reaches 0.65 mM and remains constant for the rest of the reaction time. This is because the reaction r9 is stopped after C_H reaches zero. This trend can also be observed in C_J. Finally, we can see that metabolite K is produced continuously. This can be explained by the facts that C_A is reduced to a level less than 15 mM within a few seconds and kept below 15 mM for rest of the process time.

Case 2: Flux Is Rerouted through an Alternative Pathway in a System with Feedback Inhibition on r2. Let us assume that, under certain conditions, the end product F inhibits reaction r2 in the original system according to the following equation:

$$r_2 = \frac{C_2 C_B}{C_F + C_B} \tag{8}$$

The corresponding simulation results can be found in Figure 17. It can be seen that the behavior of C_A is

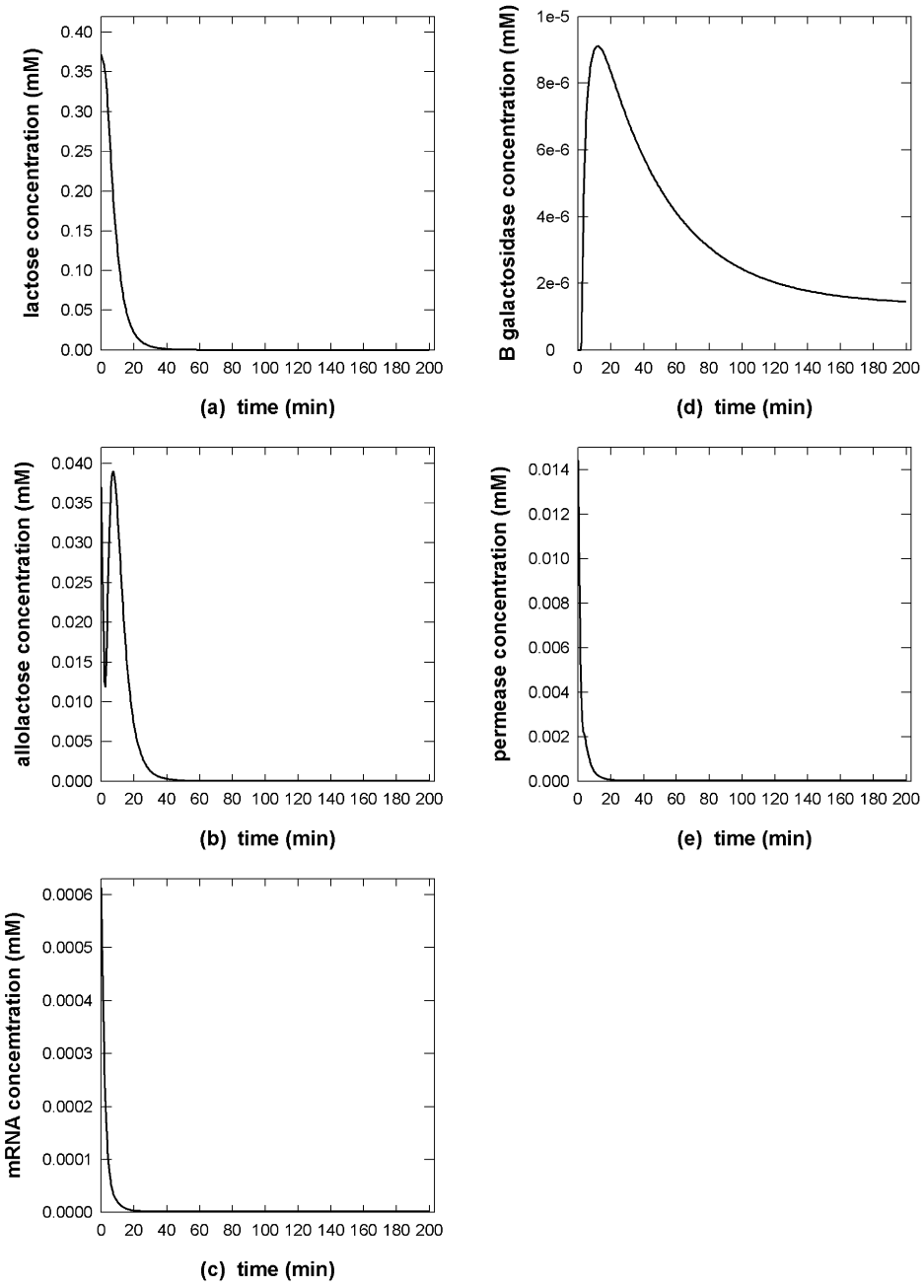

Figure 22. Simulation results obtained with Petri-net model at an initial lactose concentration of 0.008 mM: (a) internal lactose, (b) allalactose, (c) mRNAz, (d) β-galactosidase, and (e) permease.

similar to that observed in the original case (see Figure 15a). After the concentration of B increases to 3.5 mM, C_B then reduces and fluctuates around 1 mM. The increase of C_B in the initial stage may be due to the fact that C_C is quickly increased to above 1 mM and r6 is suppressed before the feedback inhibition on r2 becomes effective. The decrease of C_B later can be attributed to the fact that r6 is activated again when the feedback mechanism takes effect. Consequently, C_C is reduced to 0.25 mM after reaching a maximum at around 30 s and remains the same for the rest of reaction period. The same trends can also be observed in C_D and C_E. Notice that, although the flux via r2 is suppressed, enough flux can still be generated via r9, r10, and r11 to maintain a finite level of C_C, C_D, and C_E. Notice that the behavior of C_F is similar to that of the corresponding results obtained in the original system (see Figure 15f). The concentration of G (or H) reaches 0.5 mM (or 0.25 mM) and then fluctuates for the rest of the period. On the other hand, C_I is increases gradually with process time. This may be due to fact that the flux through r7 is higher than that through r9. The same trend can also be found in C_J. This phenomenon can be attributed to the flux difference between r9 and r10. Notice the behavior of C_K is the same as those found in the original case also (see Figure 15k). For the sake of brevity, an analysis of its causes is not repeated here. Finally, notice that the auxiliary metabolites C_X and C_Y are again similar to those observed in the original case.

As stated earlier, the gene control mechanism can be altered to improve the reaction performance. In certain applications, the desired product could be an intermediate in the reaction network. Let us assume that intermediate I is the desired product in this case. Based on

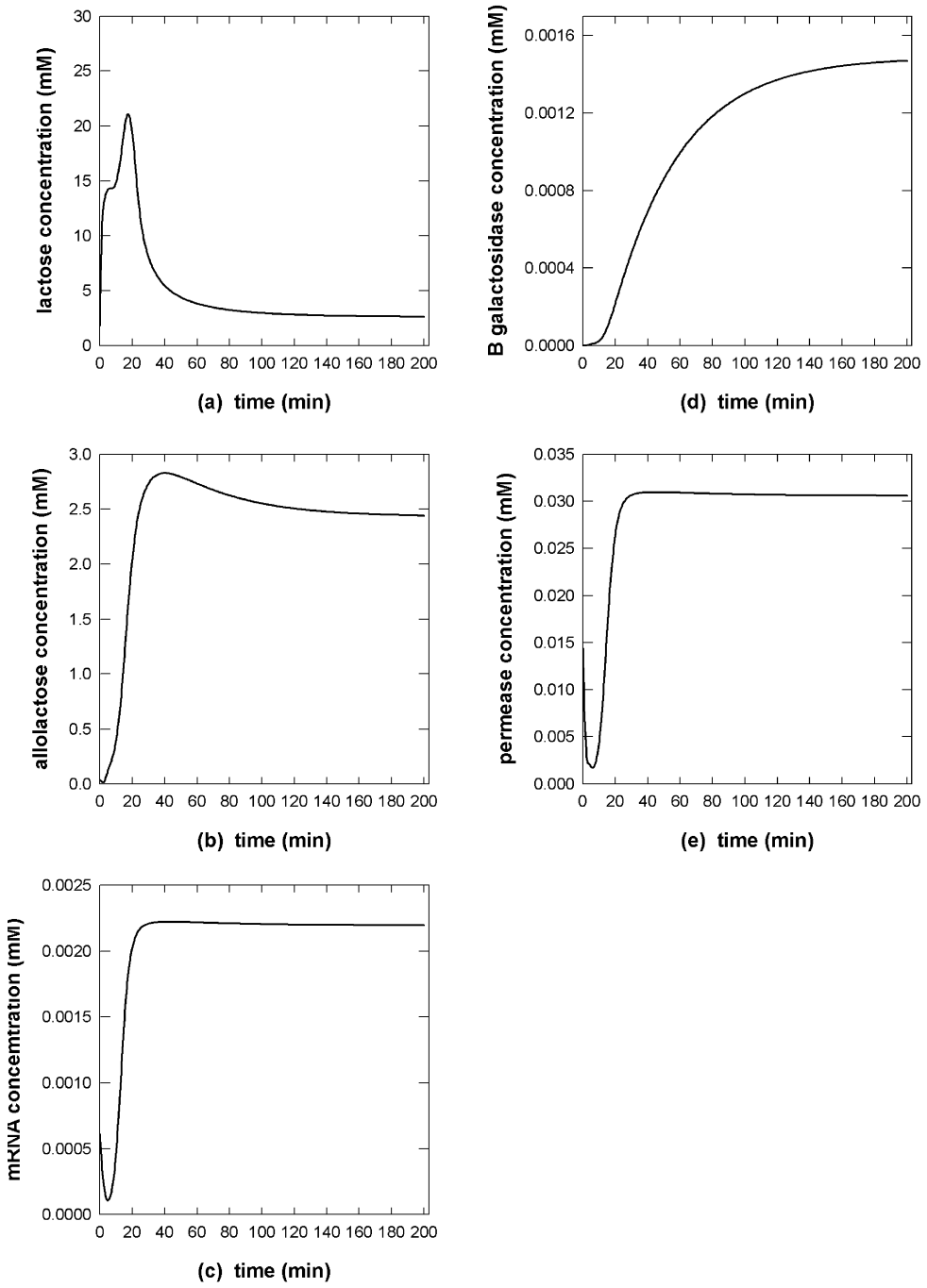

Figure 23. Simulation results obtained with Petri-net model at an initial lactose concentration of 10mM: (a) internal lactose, (b) allalactose, (c) mRNAz, (d) β-galactosidase, and (e) permease.

the simulation results presented in Figure 17, it can be concluded that reaction r8 should be halted in order to enhance the production rate of I. Accordingly, an additional regulon control mechanism (*Reg_5*) has been adopted to turn *off* the constitutive operon *Ope_c7* when C_B is above zero. The corresponding simulation results can be found in Figure 18. Notice that the trends of C_A-C_E are similar to those observed in Figure 17. The metabolites C, D, and E are formed initially and consumed completely later. This is due to the fact that r2 is suppressed by feedback inhibition mechanism and r8 is deactivated through the modified gene regulation mechanism. The metabolites H and J cannot be produced since r8 is deactivated. By comparing Figures 17i and 18i, it can be seen that a 5-fold increase in the production rate of metabolite I can be anticipated with the proposed change in the regulatory mechanism.

11. Application to a Specific Metabolic Network

To validate the proposed approach, the simulation results obtained with the Petri-net models of the *lac* operon have been compared with experimental data reported in the literature. Yildirim and Mackey[39] developed a mathematical model for describing the inductive regulation behaviors in the *lac* operon. This dynamical model takes into account of the roles of the permease (which facilitates the internalization of external lactose), internal lactose, β-galactosidase (which

is involved in the conversion of lactose to allolactose, glucose and galactose), allolactose (which interacts with the lac repressor) and mRNA (which is synthesized from structural gene via transcription). The model formulation consists of five nonlinear differential equations incorporating the time delays due to DNA transcription and mRNA translation. The Petri-net model of the *lac* operon was first assembled with these equations on the basis of Figure 6. We have tested this model with two sets of β-galactosidase activity-versus-time data. The first data set is adopted from the experimental work presented in Knorre.[40] In this study, the concentration of β-galactosidase was periodically measured after a sudden switch from the original glucose-rich and lactose-free medium to a glucose-free and lactose-rich medium for *E. coli* ML30. The second data set is taken from Pestka et al.[41] They studied the inhibition phenomena in mRNA translation process for producing β-galactosidase and published its activity-versus-time data for *E. coli* 294 in the presence of isopropylthiogalactoside (IPTG). These two data sets and the model simulation results are shown in Figure 19. For comparison purpose, the experimental and simulation data are scaled so that the steady-state β-galactosidase activities in the above three cases all reach the same value. It can be observed in Figure 19 that there is a good agreement between the trend in model predictions and that in the experimental data. As a third test, the simulation results were compared with the experimental data obtained from Goodwin.[42] In this paper, the dynamic behavior of β-galactosidase was studied in chemostat culture by feeding phosphate at constant time intervals. The length of this time interval equals the bacterial doubling time. Experimentally, it was observed that β-galactosidase concentration oscillated with the same period, i.e., the feeding time interval. Figure 20 shows the experimental data of β-galactosidase as well as the simulation results. Again, the model predictions in this case are quite reasonable.

With the above Petri-net model, we can further investigate how the concentration of external lactose (L_e) affects the induction of the lactose operon. In the first simulation run, the initial conditions were set to be the same as those used in Figure 19 (L_e = 0.08 mM). In Figure 21a−e, the concentration profiles of intracellular lactose, allolactose, mRNA, β-galactosidase, and permease are plotted, respectively. It can be observed that a net amount of intracellular lactose was consumed until a threshold amount of permease was synthesized (Figure 21a). After reaching a maximum concentration later on, there was a steady loss of lactose due to the reactions producing allolactose, glucose, and galactose via β-galactosidase. The allolactose concentration decreased briefly and subsequently increased with time (Figure 21b). At 60 min, it reached the highest point at which the lactose operon experienced the maximum induction. The mRNA concentration was lowered initially due to a larger degradation rate and then raised to a steady-state value as a result of the increase in allolactose concentration (Figure 21c). Since the synthesis rate of β-galactosidase is dependent upon the concentration of mRNA, its concentration gradually increased from zero with time. The profile of the permease concentration (Figure 21e) is similar to that of mRNA in Figure 21c. This is due to the facts that permease was produced directly from mRNA via translation. In the next simulation run, the extracellular lactose concentration was

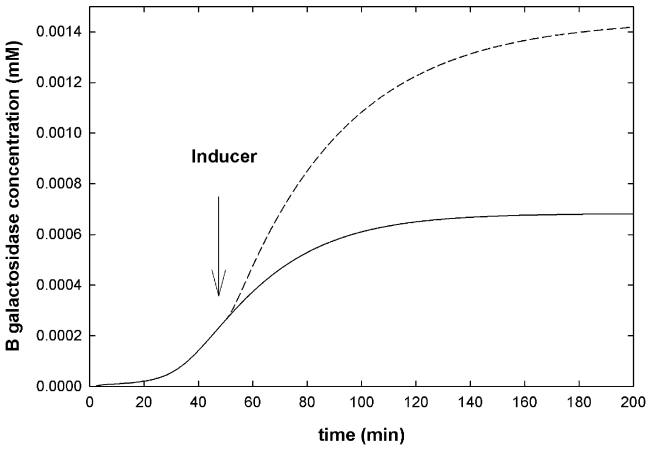

Figure 24. Qualitative simulation of the PaJaMo experiment.

decreased to 0.008 mM. It was found that the induction effects of the lactose operon were reduced drastically (see Figure 22a−e). Consequently, the concentrations of allolactose (Figure 22b) and β-galactosidase (Figure 22d) were both very low throughout the entire reaction period, and the concentrations of the other three also quickly dropped to zero (Figure 22a, c, and e). In the last case study, the concentration of external lactose concentration was raised to 10 mM. The simulation results are shown in Figure 23a−e. Notice that the steady-state β-galactosidase concentration in Figure 23d is higher than those obtained in the previous cases (see Figures 21d and 22d). This observation reflects a much more prominent induction effect.

Also, in the PaJaMo (i.e., Pardee, Jacob, and Monod) experiment, synthesis of β-galactosidase was studied during conjugation of male bacteria with female.[43] After a threshold amount of β-galactosidase was produced, enzyme synthesis stopped abruptly. If at this time additional inducer(s) can be introduced, the enzyme synthesis process could resume.[44] This phenomenon can be qualitatively reproduced with the proposed Petri-net model. Our simulation results are shown in Figure 24. At the time indicated, as a result of the added inducer (i.e., the external lactose), the production of enzyme continued (dash line). On the other hand, the enzyme level remains relatively stable without the inducer (solid line).

Finally, notice that the two important regulatory mechanisms of the *lac* operon that depend on the extracellular glucose concentration, i.e., catabolite repression and inducer exclusion, are missing in the Petri-net model used in the above case studies. It is well established that the presence of external glucose can affect the induction of expression process. In particular, the synthesis of carbohydrates is inhibited when the external glucose is plentiful. This phenomenon is known as "catabolite repression". The primary signal molecule for catabolite repression is cAMP (cyclilc AMP). In addition, the transport of lactose by permease is inhibited by external glucose, a phenomenon known as "inducer exclusion". Santillán and Mackey[45] developed a more comprehensive model of the lactose operon that includes all known regulatory mechanisms. The corresponding Petri-net model has also been constructed with the proposed approach. The model validity was again verified by simulating the experiments of Knorre.[40] The effects of varying the concentrations of external lactose

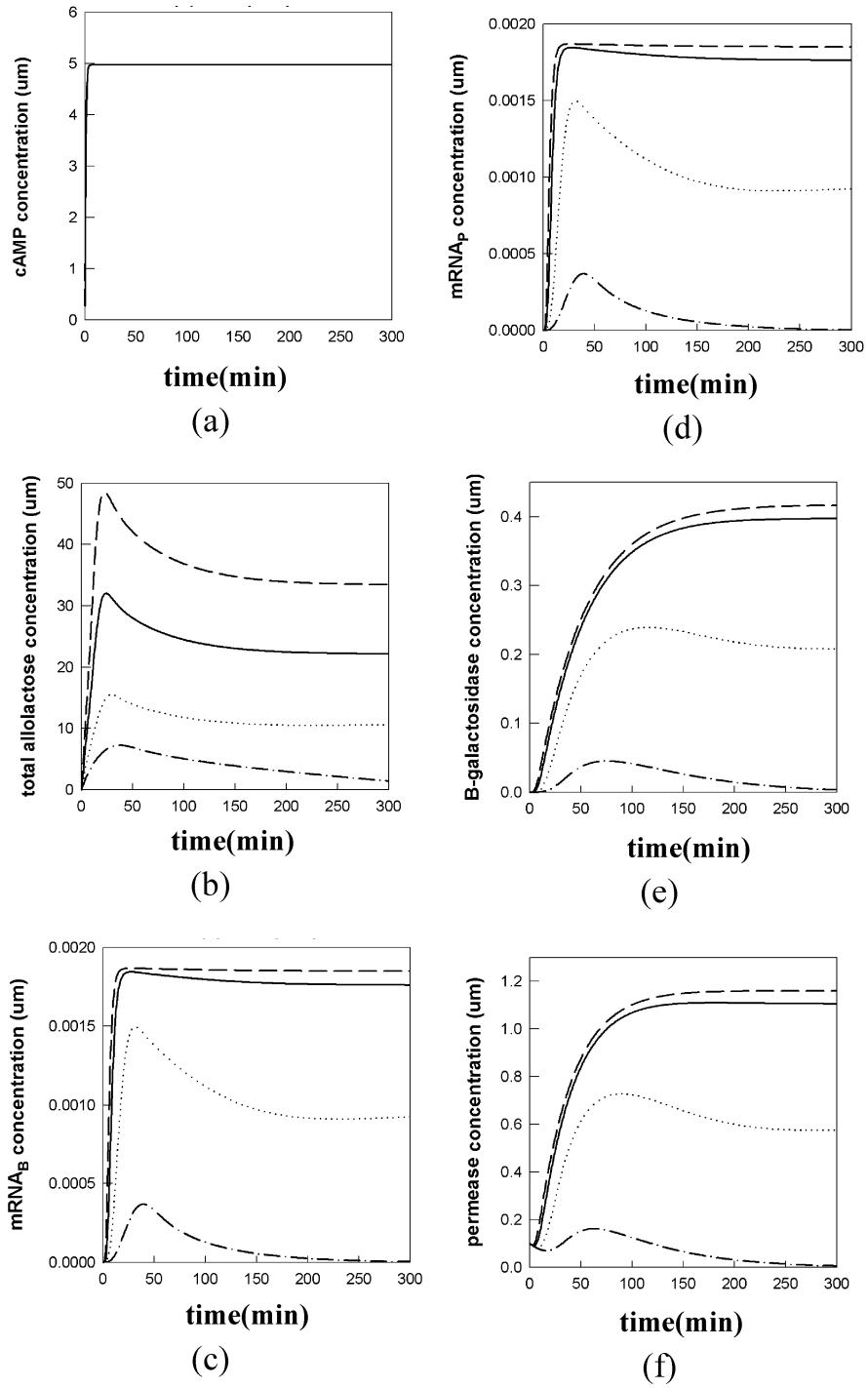

Figure 25. Simulation results obtained with Petri-net model at external lactose concentrations of 0.003 (- - -), 0.002 (—), 0.001 (· · ·), and 0.0005 mM (- · - ·) respectively: (a) cAMP, (b) allalactose, (c) $mRNA_B$, (d) $mRNA_p$, (e) β-galactosidase, and (f) permease.

and glucose on the expression process of *lac* operon can be analyzed with this more comprehensive model. In the first set of simulation runs, it can be observed that the entracellular lactose concentration does not really influence the cAMP concentration (Figure 25a). On the other hand, a higher external lactose concentration usually results in a higher lactose uptake rate and consequently causes an increase in the intracellular lactose concentration. This higher internal lactose concentration in turn drives the allolactose concentration higher (Figure 25b), and therefore the induction effect on the lactose operon becomes more pronounced. A stronger induction intensity definitely produces more $mRNA_B$ (Figure 25c), $mRNA_P$ (Figure 25d), β-galactosidase (Figure 25e), and permease concentration (Figure 25f). In the second set of simulation studies, it can be clearly seen that the presence of extracelllar glucose could inhibit the production of cAMP (Figure 26a). Lowering the cAMP concentration results in a decrease in the intracellular allolactose concentration (Figure 26b) and also weakens the induction effect. Consequently, the depletion rates of $mRNA_B$ (Figure 26c), $mRNA_P$ (Figure 26d), β-galactosidase (Figure 26e) and permease concentration (Figure 26f) become more apparent.

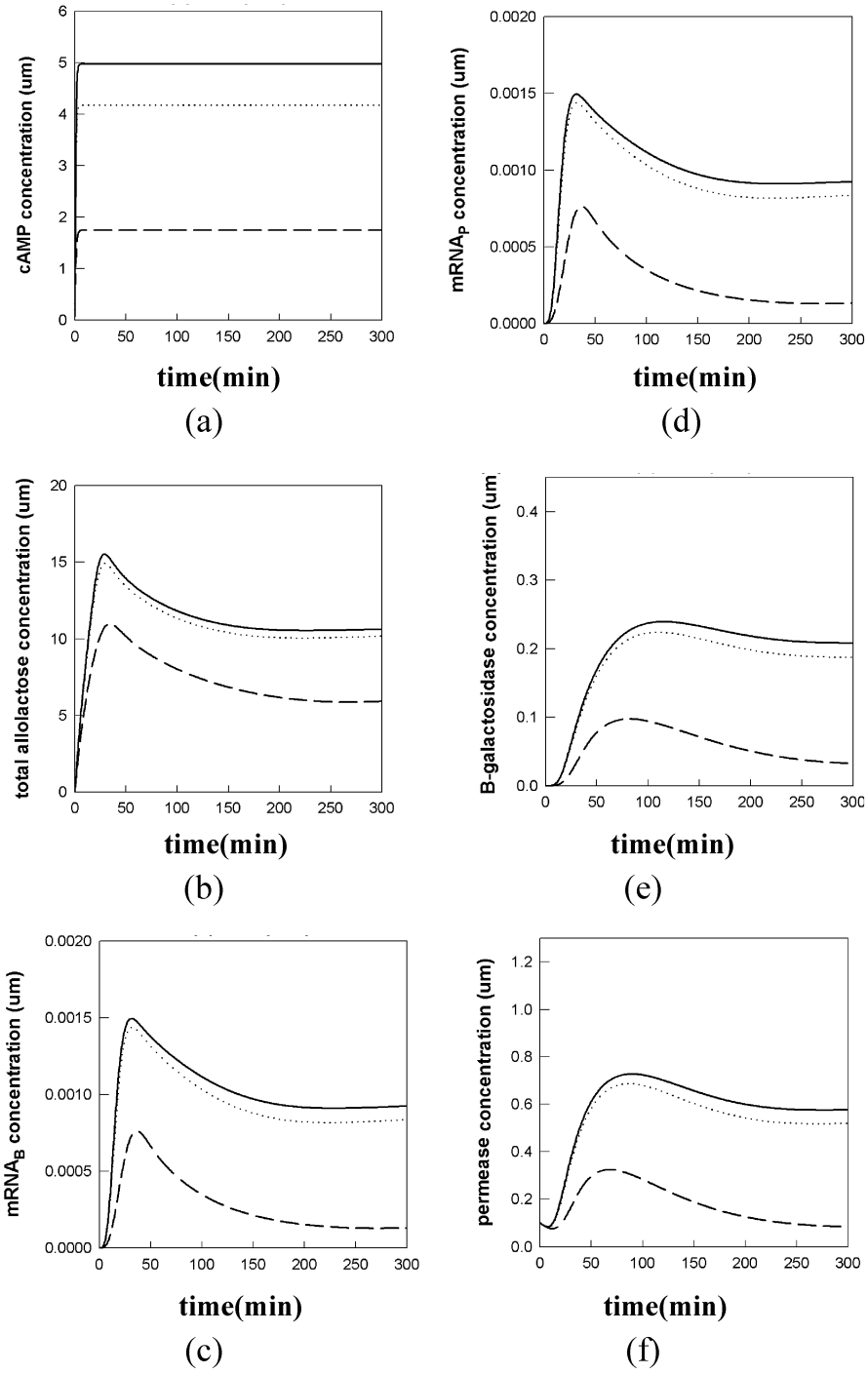

Figure 26. Simulation results obtained with Petri-net model at the external glucose concentrations of 0 (—), 10 (• • •), and 100 mM (- - -) respectively: (a) cAMP, (b) allalactose, (c) $mRNA_B$, (d) $mRNA_p$, (e) β-galactosidase, and (f) permease.

12. Conclusions

Based upon the concept of functional unit, a hierarchical approach is proposed in this study to model metabolic phenotype. Standard Petri-net models are developed to characterize the individual reactions, gene regulation mechanisms and other signal transduction processes. A systematic procedure for constructing the system models from these components is presented and also illustrated with a realistic example. The proposed approach has also been validated with experimental data. It can be observed that the metabolic systems can indeed be properly modeled with Petri nets and the required modeling load can be effectively relieved by the use of the general purpose Petri-net objects.

Nomenclature

C = concentration
C_C = enzyme concentration
C_{CI} = concentrations inside the cell
C_{CO} = concentrations outside the cell
C_I = inhibitor concentration
C_{P1} = concentration of biomolecules
C_{P3} = concentration of carrier molecules
C_S = concentration of the substrate
C_X = concentration of protein molecules
D_f = diffusivity of carrier complex
d_m = membrane thickness
D_m = diffusivity
K_d = reaction constant

K_i = Michaelis constant
K_I, K_I^* = dissociation constants
r = reaction rate
r_d = rates of decomposition and self-degradation
r_f = rate of facilitated transport
r_m = rate of molecule transport across the membrane
v_1, v_2, v_3 = maximum reaction rate

Literature Cited

(1) Bailey, J. Toward a science of Metabolic Engineering. *Science* **1991**, *252*, 1668−1673.

(2) Stephanopoulos, G. N.; Aristidou, A.A.; Nielsen, J. *Metab. Eng.*; Academic Press: New York, 1998.

(3) Stephanopoulos, G. N. Metabolic fluxes and metabolic engineering. *Metab. Eng.* **1999**, *1*, 1−11.

(4) Nielsen, J. Metabolic engineering. *Appl. Biotechnol.* **2001**, *55*, 263−283.

(5) Lengeler, J. Metabolic networks: a signal oriented approach to cellular models. *Biol. Chem.* **2000**, 911−920.

(6) Porro, D.; Brambilla, L.; Ranzi, B. M.; Martegani, E.; Alberghina, L. Development of metabolically engineered *Saccharomyces cerevisiae* cells for the production of lactic acid. *Biotechnol. Prog*. **1995**, *11*, 294−298.

(7) Flares, N.; Xiao, J.; Berry, A.; Bolivar, F.; Valle, F. Pathway engineering for the production of aromatic compounds in *E. coli*. *Nat. Biotechnol.* **1996**, *14*, 620−623.

(8) Millard, C.S.; Chao, V. P.; Liao, J. C.; Donnelly, M. Enhanced production of succinic acid by overexpression of phosphoenolpyruvate carboxylase in *E coli*. *Appl. Environ Microbiol*. **1996**, *62*, 1808−l810.

(9) Yang, Y. T.; Bennett, G. N.; San, K.-Y. Genetic and metabolic engineering. *Electron. J. Biotechnol.* **1998**, *1*, 1−8.

(10) Stephanopoulos, G. N. Metabolic engineering: perspective of chemical engineer. *AIChE J*. **2002**, *48*, 920−926.

(11) Varma, A.; Boesch, B. W.; Palsson, B. O. Biochemical production capabilities of *Escherichia coli*. *Biotechnol. Bioeng.* **1993**, *42*, 59−73.

(12) Varma, A.; Boesch, B. W.; Palsson, B. O. Stoichiometric interpretation of *Escherichia coli* glucose catabolism under various oxygenation rates. *Appl. Environ. Microbiol.* **1993**, *59*, 2465−2473.

(13) Hatzimanikatis, V.; Emmerling, M.; Saucer, U.; Bailey, J. E. Application of mathematical tools for metabolic design of microbial ethanol production. *Biotechnol. Bioeng.* **1998**, *58*, 154−161.

(14) Lin, X.; Floudas, C, A.; Wang, Y.; Broach, J. R. Theoretical and computational studies of the glucose signaling pathways in yeast using global gene expression data. *Biotechnol. Bioeng.* **2003**, *84* (7), 864−86.

(15) Fell, D. *Understanding the Control of Metabolism*; Portland Press Ltd., London, 1997; Chapter 5.

(16) Pissara P. N.; Nielsen J.; Bazin M. J. Pathway kinetics and metabolic control analysis of a high-yielding strain of *Fenicillium chrysogenum* during fed batch cultivations. *Biotechnol. Bioeng*. **1996,** *51*, 168−l76.

(17) Ramakrishna, R.; Edwards, J. S.; McCulloch, A.; Palsson, B. O. Flux-balance analysis of mitochondrial energy metabolism: consequences of systemic stoichiometric constraints. *Am. J. Physiol Regul. Integr. Comp. Physiol.* **2001**, *280*, R695−R704.

(18) Jamshidi, N.; Edwards, J. S.; Fahland, T.; Church, G. M.; Palsson, B. O. Dynamic simulation of the human red blood cell metabolic network. *Bioinformatics* **2001**, *17*, 286−287.

(19) Kremling, A.; Jahreis, K.; Lengeler, J. W.; Gilles, E. D. The organization of metabolic reaction networks: A signal-oriented approach to cellular models. *Metab. Eng.* **2000**, *2*, 190−200.

(20) Kremling, A.; Gilles, E. D. The organization of metabolic reaction networks: II. Signal processing in hierarchical structured functional units. *Metab. Eng.* **2001**, *3*, 138−2150.

(21) Kremling, A.; Bettenbrock, K.; Laube, B.; Jahreis, K.; Lengeler, J. W., & Gilles, E. D. The organization of metabolic reaction networks: III. Application for diauxic growth on glucose and lactose. *Metab. Eng.* **2001**, *3*, 362−379.

(22) Schuster, S.; Pfeiffer, T.; Moldenhauer, F.; Koch, I.; Dandekar, T. Exploring the pathway structure of metabolism: decomposition into subnetworks and application to *Mycoplasma pneumoniae*. *Bioinformatics* **2002**, *18*, 351−361.

(23) Reddy, V. N.; Libeman, M. N.; Mavrovouniotis, M. L. Qualitative analysis of biochemical reaction systems. *Comput. Biol. Med.* **1996**, *9*, 26−34.

(24) Hofestädt, R.; Thelen, S. Quantitative modeling of biochemical networks. **1998**, *1*, 0006. *http:/www. bioifo.de/isb/1998/01/006main/html/*

(25) Koch, I.; Schuster, S.; Heiner, M. Simulation and analysis of metabolic networks by time dependent Petri nets. *Bioinformatics* **1999**. *http://www.bioinfo.de/isb/ gcb99/ poster/koch/*

(26) Genrich, H.; Küffner, Voss, K. Executable Petri net models for the analysis of metabolic pathways. *Int. J. STTT* **2001**, *3*, 394−404.

(27) Goss, P. J. E.; Peccouds, J. Quantitative modeling of stochastic systems in molecular biology by using stochastic Petri nets. *Proc. Nat. Acad. Sci. U.S.A.* **1998**, 6750.

(28) Matsuno, H.; Doi, A.; Nagasaki, M.; Miyano, S. Hybrid Petri net representation of gene regulation network. *Proceedings of Pacific Symposium on Bio-computing*; World Scientific Publishing: River Edge, NJ, 2000; pp 338−349.

(29) Chen, M.; Hofestädt, R. Quantitative Petri-net model of gene regulated metabolic networks in the cell. *In Silico Biol.* **2003**, *3*, 0030.

(30) Peterson, J. L. *Petrinet Theory and the Modeling of Systems;* Prentice Hall: New York, 1981.

(31) David, R.; Alla, H. Petri net for modeling of dynamic systems−a survey. *Automatica* **1994**, *30* (2), 175−202.

(32) Drath, R. *Visual Object Net++,* **1998**. *http://www.daimi-.au.dk/PetriNets/tools/complete_de.html.*

(33) Bozinovski, S.; Müller, B.; Primio, F. di. *Autonomous Manufacturing Systems and Systems Software*; Report, **2000**. *http://www.gmd.de.*

(34) Matsuno, H.; Fujita, S.; Doi, A.; Hirata, Y.; Miyano, S. Genomic object net: Hybrid functional Petri net architecture for representing and simulating biopathways. **2002**. *http:*//bonsai-.ims.U-tokyo.ac.jp*/people/miyano/systembiology/GON2002.pdf.*

(35) Zybay, G.. *Biochemistry*, 2nd ed.; Macmillan: London, 1988.

(36) Todar, K. Regulation and control of metabolic activity. **2002**. *http://www.bact.wisc.edu/Bact303/Regulation.*

(37) Lee, S. B.; Bailey, J. E. Genetically structured models for lac promoter-operator function in the *E. coli* chromosome and in multicopy plasmids: lac operator function. *Biotechnol. Bioeng*. **1984**, *26*, 1372−l382.

(38) Lee, S. B.; Bailey, J. E. Genetically structured models for lac promoter-operator function in the chromosome and in multicopy plasmids: lac promoter function. *Biotechnol. Bioeng*. **1984**, *26*, 1383−l388.

(39) Yildirim, N.; Mackey, M. C. Feedback regulation in the lactose operon: a mathematical modeling study and comparison with experimental data. *Biophys. J.* **2003**, *84*, 2841−2851.

(40) Knorre, W. A. Oscillation of the rate of synthesis of β-galactosidase in *Escherichia coli* ML 30 and ML 308. *Biochem. Biophys. Res. Commun.* **1968**, *30*, 1248−1290.

(41) Pestka, S.; Daugherty B. L.; Hung V.; Hotta K.; Pestka R. K. Anti-mRNA: specific inhibition of translation of single mRNA molecules. *Proc. Natl. Acad. Sci. U.S.A.* **1984**, *81,* 7525−7528.

(42) Goodwin, B. C. Control dynamic of β-galactosidase in relation to the bacterial cell cycle. *Eur. J. Biochem.* **1969**, *10,* 515−522.

(43) Pardee A. B.; Jacob F.; Monod J. The genetic control and cytoplasmic expression of 'inducibility' in thr synthesis of β-galactosidase by *E. coli. J. Mol. Biol.* **1959**, *1,* 165−178.

(44) Ullmann, A. *Escherichia coli* lactose operon. *Encyclopedia of Life Sciences* **2001**. *http://www.els.net*

(45) Santillán, M.; Mackey, M. C. Influence of catabolite repression and inducer exclusion on the bistable behavior of the *lac* operon. *Biophys. J.* **2004**, *86*, 1282−1292.

Received for review March 23, 2004
Revised manuscript received August 9, 2004
Accepted January 21, 2005

IE049772K